Exocyst SEC3 and Phosphoinositides Define Sites of Exocytosis in Pollen Tube Initiation and Growth[1][OPEN]

Daria Bloch[2], Roman Pleskot[2], Přemysl Pejchar[2], Martin Potocký, Pavlína Trpkošová, Lukasz Cwiklik, Nemanja Vukašinović, Hasana Sternberg, Shaul Yalovsky*, and Viktor Žárský*

Department of Molecular Biology and Ecology of Plants, Tel Aviv University, Tel Aviv 69978, Israel (D.B., H.S., S.Y.); Institute of Experimental Botany, Czech Academy of Sciences, 165 02 Prague, Czech Republic (R.P., P.P., M.P., P.T., N.V., V.Ž.); J. Heyrovsky Institute of Physical Chemistry, Czech Academy of Sciences, 182 23 Prague, Czech Republic (L.C.); and Department of Experimental Plant Biology, Faculty of Science, Charles University, 128 44 Prague, Czech Republic (N.V., V.Ž.)

ORCID IDs: 0000-0003-0488-746 (P.P.); 0000-0002-3699-7549 (M.P.); 0000-0001-8523-0099 (P.T.); 0000-0002-2083-8738 (L.C.); 0000-0002-5195-9487 (H.S.); 0000-0003-3264-0005 (S.Y.); 0000-0002-5301-0339 (V.Ž.).

Polarized exocytosis is critical for pollen tube growth, but its localization and function are still under debate. The exocyst vesicle-tethering complex functions in polarized exocytosis. Here, we show that a *sec3a* exocyst subunit null mutant cannot be transmitted through the male gametophyte due to a defect in pollen tube growth. The green fluorescent protein (GFP)-SEC3a fusion protein is functional and accumulates at or proximal to the pollen tube tip plasma membrane. Partial complementation of *sec3a* resulted in the development of pollen with multiple tips, indicating that SEC3 is required to determine the site of pollen germination pore formation. Time-lapse imaging demonstrated that SEC3a and SEC8 were highly dynamic and that SEC3a localization on the apical plasma membrane predicts the direction of growth. At the tip, polar SEC3a domains coincided with cell wall deposition. Labeling of GFP-SEC3a-expressing pollen with the endocytic marker FM4-64 revealed the presence of subdomains on the apical membrane characterized by extensive exocytosis. In steady-state growing tobacco (*Nicotiana tabacum*) pollen tubes, SEC3a displayed amino-terminal Pleckstrin homology-like domain (SEC3a-N)-dependent subapical membrane localization. In agreement, SEC3a-N interacted with phosphoinositides in vitro and colocalized with a phosphatidylinositol 4,5-bisphosphate (PIP_2) marker in pollen tubes. Correspondingly, molecular dynamics simulations indicated that SEC3a-N associates with the membrane by interacting with PIP_2. However, the interaction with PIP_2 is not required for polar localization and the function of SEC3a in Arabidopsis (*Arabidopsis thaliana*). Taken together, our findings indicate that SEC3a is a critical determinant of polar exocytosis during tip growth and suggest differential regulation of the exocytotic machinery depending on pollen tube growth modes.

[1] This work was supported by the Czech Grant Agency (grant no. GACR 13–19073S to M.P.), the Israel Science Foundation (grant nos. ISF 827/15 and ISF–NCSF 1125/13), the Israel Center for Research Excellence on Plant Adaptation to Changing Environment (grant no. I–CORE 757–12), and the Manna Center for Plant Research at Tel Aviv University.

[2] These authors contributed equally to the article.

* Address correspondence to shauly@tauex.tau.ac.il and zarsky@ueb.cas.cz.

The author responsible for distribution of materials integral to the findings presented in this article in accordance with the policy described in the Instructions for Authors (www.plantphysiol.org) is: Shaul Yalovsky (shauly@tauex.tau.ac.il).

D.B., R.P., P.P., M.P., S.Y., and V.Ž. designed research; D.B. carried out the genetic analysis of Arabidopsis *sec3a* and *sec3b* mutants, analyzed the protein localization in Arabidopsis pollen tubes, and analyzed the immunolocalization of pectin in Arabidopsis pollen tubes; R.P. and L.C. carried out the molecular dynamics simulation, structural modeling, and phylogenetic analysis; R.P., P.P., M.P., P.T., and N.V carried out the protein-lipid interaction assays, analyzed protein localization in tobacco pollen tubes, and created plasmids; H.S. created plasmids; D.B., R.P., P.P., M.P., N.V., H.S., S.Y., and V.Ž. analyzed data; D.B., R.P., P.P., M.P., S.Y., and V.Ž. wrote the paper.

[OPEN] Articles can be viewed without a subscription.

www.plantphysiol.org/cgi/doi/10.1104/pp.16.00690

Pollen tube growth provides a unique model system for studying the role of exocytosis in cell morphogenesis. Pollen tubes are characterized by a highly rapid polarized unidirectional tip growth. Given the relative simplicity of their structure, fast growth rates, haploid genome content, and ability to grow under in vitro culture conditions, pollen tubes provide an extremely attractive system for studying cell morphogenesis. Furthermore, the growth characteristics of pollen tubes resemble those of root hairs, moss protonema, and fungal hyphae and to some extent can be paralleled to neurite growth (Chebli and Geitmann, 2007; Cheung and Wu, 2008; Guan et al., 2013; Hepler and Winship, 2015).

It is well established that oscillating polarized exocytosis is fundamental for pollen tube development and determines growth rate (Bove et al., 2008; McKenna et al., 2009; Chebli et al., 2013). Exocytosis is required for the delivery of membrane and cell wall components to the growing tip. Yet, the exact location where exocytosis takes place is under debate. Ultrastructural studies showing the accumulation of vesicles at the tip suggested that exocytosis takes place at the tip (Lancelle

et al., 1987; Lancelle and Hepler, 1992; Derksen et al., 1995), which was further supported by studies on the dynamics of cell wall thickness (Rojas et al., 2011), secretion of pectin methyl esterase (PME) and PME inhibitor, and staining of pectin by propidium iodide (PI; Röckel et al., 2008; Rounds et al., 2014). Conversely, based on colabeling with FM1-43 and FM4-64, it was concluded that exocytosis takes place in a subapical collar located in the transition zone between the tip and the shank, as well as at the shank, but not at the tip (Bove et al., 2008; Zonia and Munnik, 2008). In agreement, the pollen tube-specific syntaxin GFP-SYP124 was observed in the inverted cone, 10 to 25 μm away from the tip (Silva et al., 2010), and fluorescence recovery after photobleaching experiments with FM dyes also have indicated that exocytosis takes place at the subapical region (Bove et al., 2008; Moscatelli et al., 2012; Idilli et al., 2013). Yet, based on pollen tube reorientation experiments in a microfluidics device, it was concluded that growth takes place at the tip rather than at a subapical collar located in the transition zone between the apex and the shank (Sanati Nezhad et al., 2014). The tip-based growth is in agreement with exocytosis taking place at the tip. Presumably, part of the disagreement regarding the site of exocytosis resulted from the lack of intracellular markers for exocytosis (Cheung and Wu, 2008; Hepler and Winship, 2015), and as a result, the relationship between the FM dye-labeled inverted cone and exocytotic events during pollen tube growth is not fully understood.

In many cell types, the process of secretory vesicles tethering and docking prior to fusion with the plasma membrane is initially mediated by an evolutionarily conserved tethering complex known as the exocyst. The exocyst is a heterooligomeric protein complex composed of eight subunits, SEC3, SEC5, SEC6, SEC8, SEC10, SEC15, EXO70, and EXO84 (TerBush et al., 1996; Guo et al., 1999). Studies originally based on budding yeast (*Saccharomyces cerevisiae*) have shown that the exocyst functions as an effector of Rab and Rho small GTPases that specifies the sites of vesicle docking and fusion at the plasma membrane in both space and time (Guo et al., 2001; Zhang et al., 2001). Support for the function of the exocyst in vesicle tethering was demonstrated recently by ectopic Sec3p-dependent vesicle recruitment to the mitochondria (Luo et al., 2014).

Land plants contain all subunits of the exocyst complex, which were shown to form the functional complex (Elias et al., 2003; Cole et al., 2005; Synek et al., 2006; Hála et al., 2008). Studies in Arabidopsis (*Arabidopsis thaliana*) and maize (*Zea mays*) have implicated the exocyst in the regulation of pollen tube and root hair growth, seed coat deposition, response to pathogens, cytokinesis, and meristem and stigma function (Cole et al., 2005; Synek et al., 2006; Hála et al., 2008; Fendrych et al., 2010; Kulich et al., 2010; Pecenková et al., 2011; Safavian and Goring, 2013; Wu et al., 2013; Safavian et al., 2015; Zhang et al., 2016). The growth arrest of pollen tubes in *sec8*, *sec6*, *sec15a*, and *sec5a/sec5b* single and double mutants (Cole et al., 2005; Hála et al., 2008) or following treatment with the EXO70 inhibitor ENDOSIDIN2 (Zhang et al., 2016), and of root hairs in maize *root hairless1* (*rth1*) *SEC3* mutant (Wen et al., 2005), the inhibition of seed coat deposition in the *sec8* and *exo70A1* mutants (Kulich et al., 2010), and stigmatic papillae function in *exo70A1* mutant plants (Safavian and Goring, 2013; Safavian et al., 2015) have implicated the exocyst in polarized exocytosis in plants. Given their function, it was likely that exocyst subunits could be used as markers for polarized exocytosis. Furthermore, it could also be hypothesized that, by studying the mechanisms that underlie the association of the exocyst complex with the plasma membrane, it should be possible to identify mechanisms underlying the regulation of polarized exocytosis (Guan et al., 2013). Moreover, since the interaction of exocytotic vesicles with the exocyst is transient and marks the site(s) of active exocytosis in the membrane, fluorescently labeled exocyst subunits could be used as markers for exocytosis while avoiding potential imaging artifacts stemming from pollen tube tips densely populated with vesicles.

We have shown previously that the ROP effector ICR1 can interact with SEC3a and that ROPs can recruit SEC3a-ICR1 complexes to the plasma membrane (Lavy et al., 2007). However, ICR1 is not expressed in pollen tubes, suggesting that SEC3a membrane binding in these cells is likely dependent on other factors. In yeast, the interaction of Sec3p and Exo70p subunits with the plasma membrane is critical for exocyst function (He and Guo, 2009). It has been shown that the membrane binding of both Sec3p and Exo70p is facilitated by their interaction with phosphatidylinositol 4,5-bisphosphate (PIP_2; He et al., 2007; Zhang et al., 2008). The yeast Exo70p interacts with PIP_2 via a number of positively charged residues distributed along the protein, with the highest number located at the C-terminal end (Pleskot et al., 2015). It has been suggested that yeast Sec3p interacts with PIP_2 through N-terminal basic residues (Zhang et al., 2008). These data were further corroborated by x-ray crystallography studies, which showed that the yeast Sec3p N-terminal region forms a Pleckstrin homology (PH) domain fold (Baek et al., 2010; Yamashita et al., 2010), a PIP_2 interaction motif (Lemmon, 2008).

The localization of the exocyst subunits has been addressed in several studies. In Arabidopsis root hairs and root epidermis cells, SEC3a-GFP was observed in puncta distributed throughout the cell (Zhang et al., 2013). Studies on the Arabidopsis EXO70 subunits EXO70E2, EXO70A1, and EXO70B1 revealed them to be localized in distinct compartments that were termed exocyst-positive organelles (Wang et al., 2010). The exocyst-positive organelles, visualized mostly by ectopic expression, were shown to be cytoplasmic double membrane organelles that can fuse with the plasma membrane and secrete their contents to the apoplast in an exosome-like manner. It is not yet known whether other exocyst subunits also are localized to the same organelles and what might be the biological function of

this putative compartment (Wang et al., 2010; Lin et al., 2015). In differentiating xylem cells, two coiled-coil proteins termed VESICLE TETHERING1 and VESICLE TETHERING2 recruit EXO70A1-positive puncta to microtubules via the GOLGI COMPLEX2 protein (Oda et al., 2015). Importantly, the functionality of the XFP fusion proteins used for the localization studies described above was not tested, and in most cases, the fusion proteins were overexpressed. Therefore, the functional localization of the exocyst is still unclear.

Here, we studied the function and subcellular localization of the Arabidopsis exocyst SEC3a subunit using a combination of genetics, cell biology, biochemistry, and structural modeling approaches. Our results show that SEC3a is essential for the determination of pollen tube tip germination site and growth. Partial complementation of *sec3a* resulted in the formation of pollen with multiple pollen tube tips. In Arabidopsis growing pollen tubes, SEC3a localization is dynamic, and it accumulates in domains of polarized secretion, at or close to the tip plasma membrane (PM). Labeling of GFP-SEC3-expressing pollen with FM4-64 revealed the spatial correlation between polarized exocytosis and endocytic recycling. Furthermore, the association of SEC3a with PM at the tip marks the direction of tube elongation and positively correlates with the deposition of PI-labeled pectins and specific anti-esterified pectin antibodies in the cell wall. In tobacco (*Nicotiana tabacum*), the mechanisms underlying SEC3a interaction with the PM and its subcellular distribution depend on pollen tube growth mode and involve the interaction with PIP2 through the N-terminal PH domain. Collectively, our results highlight the function of SEC3a as a polarity determinant that links between polarized exocytosis and cell morphogenesis. The correlation between exocyst function and distribution in pollen tubes provides an explanation for some of the current discrepancies regarding the localization of exocytosis.

RESULTS

Expression of SEC3 Paralogs in Arabidopsis

In Arabidopsis, there are two *SEC3* paralogs, *SEC3a* (*At1g47550*) and *SEC3b* (*At1g47560*), encoded as a tandem duplication in the genome and showing 84% and 97% nucleotide identity in their genomic and coding sequences, respectively (Cvrčková et al., 2012). The high degree of sequence identity between *SEC3a* and *SEC3b* delayed their correct annotation (Lamesch et al., 2012) and compromised the determination of their expression patterns by microarrays. Reliable expression data for each of the two genes could be obtained only using oligonucleotide primers for the 3′ untranslated region (Supplemental Fig. S1). The expression patterns of *SEC3a* and *SEC3b* were determined by reverse transcription (RT)-PCR. The *SEC3a* transcript was detected in seedlings, roots, and different organs of the sporophyte, including flowers (Fig. 1A). GUS expression driven by the *SEC3a* promoter confirmed the constitutive expression pattern detected by RT-PCR and further indicated that the expression of *SEC3a* is higher in primary root tips, distal tips of cotyledons, and lateral root primordia (Fig. 1, B–D). Compared with *SEC3a*, *SEC3b* expression was much lower and spatially restricted, with low transcript levels that could be detected only in flowers and siliques (Fig. 1A). Within flowers, *SEC3a* and *SEC3b* expression was detected in ovules, fully developed anthers, and in vitro-germinated pollen (Fig. 1A). The expression and promoter analysis suggested that *SEC3a* is the major SEC3 paralog in Arabidopsis and that *SEC3b* may function redundantly with *SEC3a* in some floral tissues.

Identification of T-DNA Insertion Mutants in SEC3a and SEC3b

To analyze the function of SEC3 in Arabidopsis, we employed a reverse genetics approach. To this end, we identified T-DNA insertion mutants in both *SEC3a* and *SEC3b*. The GABI_652H12 line carries a T-DNA insertion in the last exon, namely exon 25, of the *SEC3a* gene (*sec3a-1*), and the SALK_064295 line carries a T-DNA insertion in exon-17 of *SEC3b* (*sec3b-1*; Fig. 1E). Exact positions of the T-DNA inserts and fitting of the insert to the specific paralog were verified by sequencing (Supplemental Fig. S1B). It is important to mention that we also analyzed additional *SEC3a* mutant alleles (SALK_140590, SALK_145185, and SALK_140593, all predicted to carry an insert in the first intron), but we were unable to identify T-DNA inserts at the predicted locations, suggesting incorrect annotations of these lines.

The *sec3a-1* allele shows resistance to the sulfadiazine (Sd) selection marker, which cosegregates with the T-DNA insert in *SEC3a*. Homozygous *sec3a-1*$^{-/-}$ plants could not be obtained from heterozygote *sec3a-1* progeny (Table I; Supplemental Fig. S2, A and B). Moreover, the progeny of *sec3a-1*$^{+/-}$ heterozygote plants segregated at a 1:1 ratio with respect to Sd resistance, deviating from the expected 3:1 Mendelian segregation ratio (Table II), thus implying a gametophytic transmission defect. In contrast to *sec3a-1*, homozygous *sec3b-1*$^{-/-}$ plants were identified using a combination of *SEC3b* gene-specific and T-DNA-specific primers (Supplemental Fig. S2C). The *SEC3b* mRNA transcript could not be detected in *sec3b-1*$^{-/-}$ homozygous flowers, indicating that *sec3b-1* is a null allele (Fig. 1F). The macroscopic phenotype of *sec3b-1*$^{-/-}$ homozygous seedlings is similar to that of wild-type Col-0 (Supplemental Fig. S3), which is not surprising, given the low expression levels of *SEC3b* and its redundancy with *SEC3a*.

Pollen-Specific Transmission Defects in *sec3a-1*

The *sec3a-1* heterozygote plants were outcrossed to wild-type Col-0 plants for three successive generations to reduce the chance of nonrelated mutations linked to the allele, and they always segregated at a 1:1 ratio with respect to Sd resistance. In order to verify whether

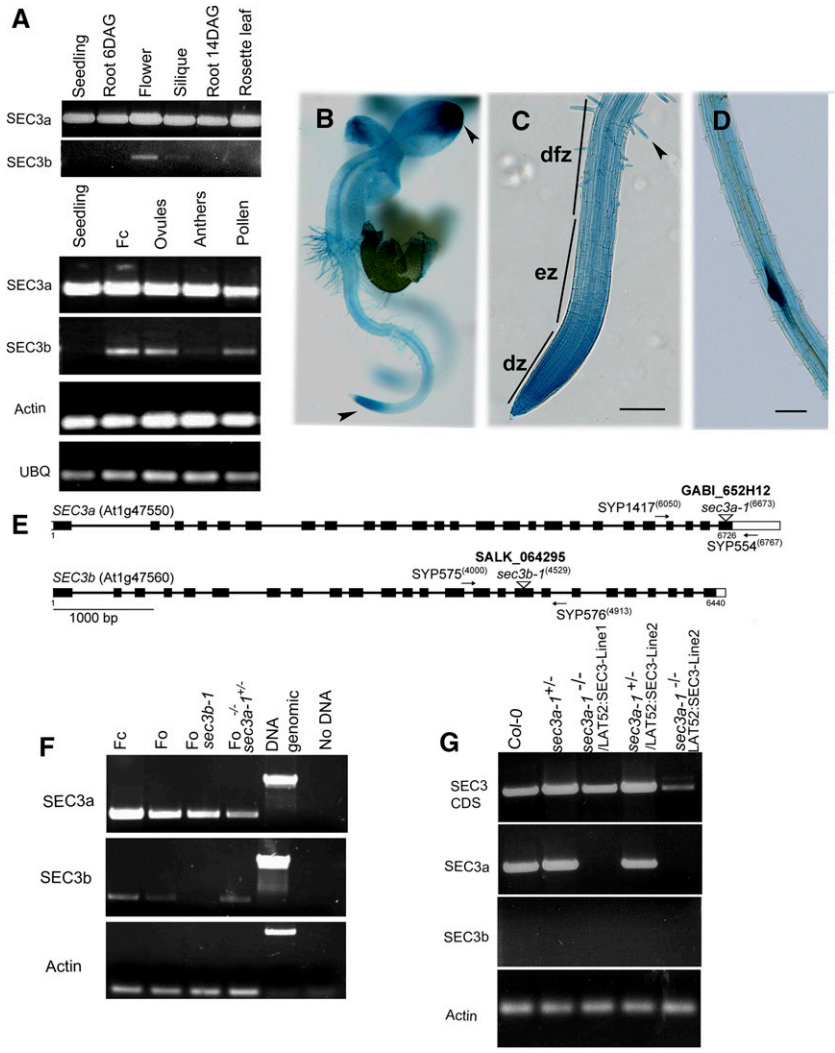

Figure 1. Expression pattern of the *SEC3a* and *SEC3b* paralogs and genotyping of *sec3a-1* and *sec3b-1* mutants. A, RT-PCR showing the expression of *SEC3a* and *SEC3b* in seedlings at 6 and 14 d after germination (DAG), different mature plant organs, closed flowers (Fc), ovules, anthers (fully developed from closed flowers), and in vitro-germinated pollen. B to D, Expression pattern of *SEC3a* (*PSEC3a*:*GUS*) in seedlings. Four independent lines were used for analysis. B, A 2-DAG seedling showing the highest expression levels in cotyledons and primary root tips (arrowheads). C, A primary root of a 2-DAG seedling. dfz, Differentiation zone; dz, division zone; ez, elongation zone. The arrowhead marks expression in root hairs. D, A root with an emerging lateral root primordium. Bars = 50 μm. E, Schematic representation of *SEC3a* and *SEC3b* gene exon-intron organization. Gene-specific primers used for genotyping and determining the T-DNA insert locations are specified by arrows. Numbers indicate nucleotide positions from the initiation ATG codon. The T-DNA inserts at positions 6,673 in *SEC3a* and 4,529 in *SEC3b* are highlighted by arrowheads. F, RT-PCR showing the expression of *SEC3a* and *SEC3b* in flowers of the indicated genotypes. Fo, Open flower. A genomic DNA control was included to display primer efficiency. G, *SEC3a* and *SEC3b* expression in *sec3a-1*/*LAT52*:*SEC3a* complemented plants. Note that in *sec3a-1*$^{-/-}$/*LAT52*:*SEC3a* homozygous lines, expression of the *SEC3a* coding sequence (CDS) indicates that the *SEC3a* transgene construct was in the sporophyte (for primer details, see Supplemental Fig. S1).

transmission defects in *sec3a-1*$^{+/-}$ plants are associated with the male or the female gametophyte, reciprocal outcrosses to Col-0 were performed. When *sec3a-1*$^{+/-}$ pollen was used for fertilization of the wild type, the mutant allele was not transferred to the progeny (n = 408), whereas in reciprocal crosses, the mutant allele was transmitted at the predicted ratio (n = 483). These data indicate that the *sec3a-1* allele has a male gametophyte transmission defect (Table II).

To confirm that the pollen-transmission defects in the *sec3a-1* allele were associated with the mutation in *SEC3a*, gene complementation experiments were performed. Plants expressing the coding sequence of SEC3a and of SEC3a N-terminally fused to GFP (GFP-SEC3a) under the control of the pollen promoter *LAT52* were crossed to the *sec3a-1* heterozygote plants, thus generating *sec3a-1*$^{+/-}$/*LAT52*:*SEC3a* and *sec3a-1*$^{+/-}$/*LAT52*:*GFP-SEC3a* plants, respectively. Outcrosses to

Table I. *Genotyping and segregation analysis of self crosses in* sec3a-1 *mutant and complementation lines*

Shown is a summary of genotypes detected in Sd-resistant progeny of *sec3a-1*$^{+/-}$, *sec3a-1*$^{+/-}$/*LAT52*:*SEC3a*, and *sec3a-1*$^{+/-}$/*LAT52*:*GFP-SEC3a* complementation lines, confirmed by PCR analysis. The χ^2 test was applied for statistical analysis: $P \leq 0.005$ indicates that observed data differ significantly from the expected data; NS, not significantly different.

Genotype	N	sec3a-1$^{+/-}$	sec3a-1$^{-/-}$	χ2	P
sec3a-1$^{+/-}$ (self-cross)	72	72	0	36	≤0.0001
sec3a-1$^{+/-}$/*LAT52*:*SEC3a* line 1$^{+/-}$	8	5	3	0.063	≥0.80, NS
sec3a-1$^{+/-}$/*LAT52*:*SEC3a* line 2$^{+/-}$	23	21	2	6.283	≥0.01
sec3a-1$^{+/-}$/*LAT52*:*GFP-SEC3a* line1$^{+/-}$	12	9	3	0.375	≥0.5, NS
Expected		66.6%	33.3%		

Table II. *Genotyping and segregation analysis of reciprocal outcrosses in* sec3a-1 *mutant and complementation lines*

Shown is a summary of Sd-resistant and -sensitive progeny in reciprocal outcrosses of *sec3a-1*$^{+/-}$, *sec3a-1*$^{+/-}$*/LAT52*:*SEC3a*, and *sec3a-1*$^{+/-}$*/LAT52*:*GFP-SEC3a* to the Columbia-0 (Col-0) background. *, The difference from expected could be explained by the variable expression levels of the complementation constructs in individual pollen. The χ^2 test was applied for statistical analysis: $P \leq 0.005$ indicates that observed data differ significantly from the expected data; NS, not significantly different.

Reciprocal Outcrosses	Sd Selection Marker				
	N	*Sensitive +/+*	*Resistant sec3a-1*$^{+/-}$ or *sec3a-1*$^{-/-}$	χ^2	*P*
sec3a-1$^{+/-}$ (self-cross)	1,140	52%	48%	323	≤0.0001
Expected		25%	75%		
Pollen source: *sec3a-1*$^{+/-}$	408	100%	0%	408	≤0.0001
Pollen recipient: Col-0					
Pollen source: Col-0	483	50.5%	49.5%	0.033	≥0.8, NS
Pollen recipient: *sec3a-1*$^{+/-}$					
Expected		50%	50%		
Pollen source: *sec3a-1*$^{+/-}$/ *LAT52*:*SEC3a* line1$^{+/-}$	228	72%	28%	2.8	≤0.1, NS
Pollen recipient: Col-0					
Pollen source: *sec3a-1*$^{+/-}$/ *LAT52*:*GFP-SEC3a* line 1$^{+/-}$	198	80%	20%	15.3	≤0.001*
Pollen recipient: Col-0					
Pollen source: *sec3a-1*$^{+/-}$/ *LAT52*:*SEC3a KRKR/A* line 3$^{+/-}$	145	74%	26%	2.027	≥0.1, NS
Pollen recipient: Col-0					
Pollen source: *sec3a-1*$^{+/-}$/ *LAT52*:*GFP-SEC3a KRKR/A* line 4$^{+/-}$	93	68%	32%	0.048	≤0.5, NS
Pollen recipient: Col-0					
Pollen source: *sec3a-1*$^{+/-}$/ *LAT52*:*SEC3a-ΔN* line 2$^{+/-}$	182	78%	22%	10.571	≤0.001*
Pollen recipient: Col-0					
Pollen source: *sec3a-1*$^{+/-}$/ *LAT52*:*GFP-SEC3a-ΔN* line 3$^{+/-}$	127	87%	13%	22.763	≤0.001*
Pollen recipient: Col-0					
Expected		66.6%	33.3%		
Pollen source: Col-0	188	52%	48%	0.340	>0.5, NS
Pollen recipient: *sec3a-1*$^{+/-}$/ *LAT52*:*SEC3a* line2$^{+/-}$					
Pollen source: Col-0	112	51%	49%	0.036	>0.8, NS
Pollen recipient: *sec3a-1*$^{+/-}$/ *LAT52*:*GFP-SEC3a* line1$^{+/-}$					
Expected		50%	50%		

the Col-0 background indicated that both constructs successfully complemented the male gametophytic defects associated with the *sec3a-1* mutation, since the mutant allele was transmitted through the pollen and cosegregated with Basta resistance, a selection marker for *LAT52*:*SEC3a/GFP-SEC3a* lines (Table II; Supplemental Table S1). In control reciprocal outcrosses, *LAT52*:*SEC3a* and *LAT52*:*GFP-SEC3a* did not affect the transmission of the *sec3a-1* allele through the female gametophyte and did not cosegregate with the mutation (Table II; Supplemental Table S1).

Homozygous *sec3a-1*$^{-/-}$ plants were identified among the progeny of self-crossed *sec3a-1*$^{+/-}$*/LAT52*:*SEC3a* complementation lines using PCR (Table I; Supplemental Fig. S2D), which was further confirmed by nonsegregating Sd-resistant progeny (Supplemental Table S2). Endogenous *SEC3a* expression was not detected in *sec3a-1*$^{-/-}$*/LAT52*:*SEC3a* seedlings, indicating that *sec3a-1* is a null allele, while a transcript corresponding to the SEC3a coding sequence used for complementation was present in *sec3a-1*$^{-/-}$ seedlings, indicating that, in our system, the *LAT52* promoter also drove expression in the sporophyte (Fig. 1G). Moreover, *SEC3b* expression was not up-regulated in *sec3a-1*$^{-/-}$*/LAT52*:*SEC3a* seedlings. To confirm that the *sec3a-1* phenotype was not associated with embryonic lethality, we counted the number of aborted seeds and found it to be similar to that in plants without the T-DNA insert (Supplemental Table S3). Taken together, these data showed that knockout of *SEC3a* resulted in a male gametophyte transmission defect, similar to mutants in genes encoding the SEC5, SEC6, SEC8, and SEC15 exocyst subunits (Cole et al., 2005; Hála et al., 2008).

Pollen Germination and Pollen Tube Growth Are Compromised in the *sec3a-1* Mutant

Next, we examined whether the male gametophyte transmission defect in *sec3a-1* plants is due to compromised

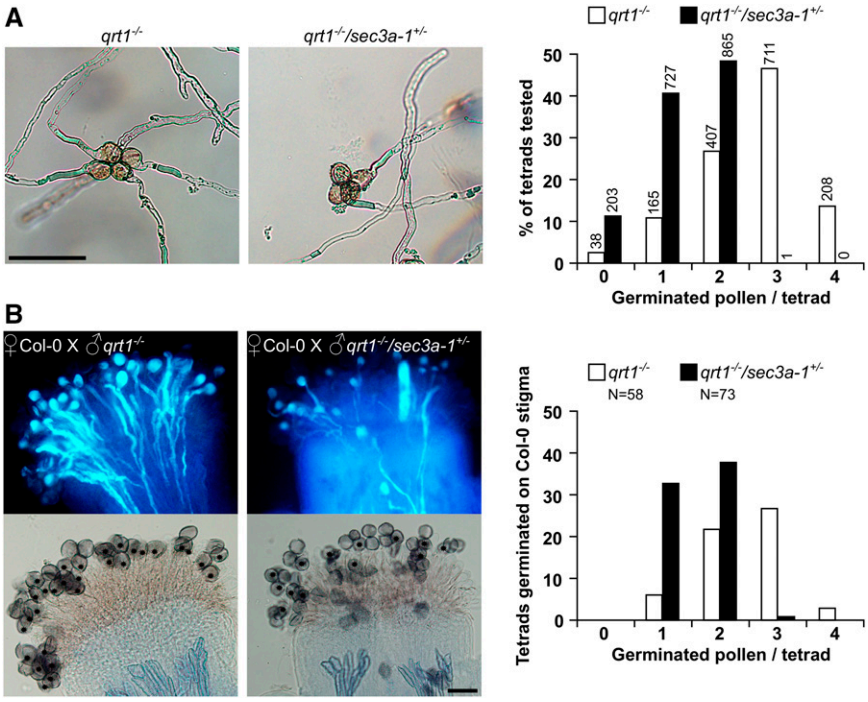

Figure 2. Tetrad analysis of *sec3a-1* heterozygotes. A, In vitro-germinated tetrads from self-crosses of $qrt1^{-/-}$ and $qrt1^{-/-}/sec3a\text{-}1^{+/-}$ plants. The chart shows the percentage from total quartets with the indicated number of germinated pollen grains in each tetrad (between zero and four) compared with the total tetrads scored for each genotype. Numbers above the bars represent actual numbers of tetrads that were counted. B, Aniline Blue staining of wild-type stigma 24 h after pollination with either $qrt1^{-/-}$ or $qrt1^{-/-}/sec3a\text{-}1^{+/-}$ tetrads. Asterisks mark germinated pollen grains in tetrads as revealed by the staining. The chart shows in vivo germination analysis of $qrt1^{-/-}$ and $qrt1^{-/-}/sec3a\text{-}1^{+/-}$ tetrads germinated on Col-0 stigma. The number of pollen tubes producing cells in each quartet (between one and four) was counted using Aniline Blue staining. Bars = 50 μm.

pollen tube growth. To this end, $sec3a\text{-}1^{+/-}$ heterozygous plants were crossed into the *quartet1* (*qrt1*) mutant background. In *qrt1*, the four meiotic products of the pollen mother cell are fused, and pollen grains are released as tetrads (Preuss et al., 1994). Heterozygous *sec3a-1* tetrads ($sec3a\text{-}1^{+/-}/qrt^{-/-}$) showed a 2:2 ratio of normal to affected pollen and allowed direct examination of the mutant phenotype. When the *qrt1* pollen was germinated in vitro, approximately 60% of all tetrads (n = 1,529) had three to four pollen grains with germinated long pollen tubes. In *sec3a-1* heterozygous tetrads (n = 1,769), only one or two cells formed pollen tubes, and the other cells either did not germinate or produced small protrusions that did not elongate (Fig. 2A).

To further confirm that male transmission defects in $sec3a\text{-}1^{+/-}$ plants were associated with pollen tube growth, in situ germination experiments were performed. Pollen from $sec3a\text{-}1^{+/-}/qrt^{-/-}$ (n = 73) and $qrt^{-/-}$ (n = 58) plants were used to pollinate wild-type Col-0 stigma, and 24 h after germination, the plants were stained with Aniline Blue, which stains the callose in the pollen tube cell wall. As expected from the in vitro germination experiments, 72 of 73 *sec3a-1* heterozygous tetrads germinated only one to two pollen tubes, compared with more than 50% of tetrads with three to four pollen tubes in *qrt1* (Fig. 2B).

To test whether the loss of *SEC3a* function does affect early stages of microspore and pollen development, nuclei of mature tetrads were stained with 4′,6-diamidino-2-phenylindole (DAPI). One vegetative nucleus and two sperm cell nuclei were detected in each pollen grain of $qrt^{-/-}$ and $qrt^{-/-}/sec3a\text{-}1^{+/-}$ tetrads, indicating that the loss of *SEC3a* function does not affect mitosis during male gametogenesis (Supplemental Fig. S4). Collectively, our results indicate that, similar to other exocyst complex subunits, *SEC3a* function is required for the proper germination of pollen grains and subsequent pollen tube growth.

SEC3a Polar Localization at the Tip Is Dynamic and Predicts the Growth Direction in the Arabidopsis Pollen Tube

Given that mutation in the *SEC3a* gene led to pollen transmission defects and that the GFP-SEC3a fusion protein complemented the mutant phenotype, we next focused on the localization of SEC3a in Arabidopsis pollen tubes. In transgenic plants expressing *LAT52*:*GFP-SEC3a*, enrichment of the GFP-SEC3a signal was detected at the apical region of growing pollen tubes (Fig. 3A). Imaging of a middle section of the pollen tube apex with the pinhole set to 1 Airy unit revealed the presence of a polar fraction of GFP-SEC3a localized to the tip appearing as thin lines at or near the PM (Fig. 3B). Conversion of the GFP signal to a range of intensities uncovered that GFP-SEC3a also forms a subapical inverted cone (Fig. 3C). Next, we utilized time-lapse imaging to follow the dynamics of GFP-SEC3a polar localization in elongating Arabidopsis pollen tubes. Under our experimental conditions, pollen tubes elongated with a rate of 3.5 to 4 μm min^{-1} and occasionally changed the direction of growth, suggesting a correlation between GFP-SEC3a localization and the direction of pollen tube growth. In elongating pollen tubes, the polar fraction of GFP-SEC3a close to the tip PM was highly dynamic and shifted its position toward the future growth axis before visible changes in the direction

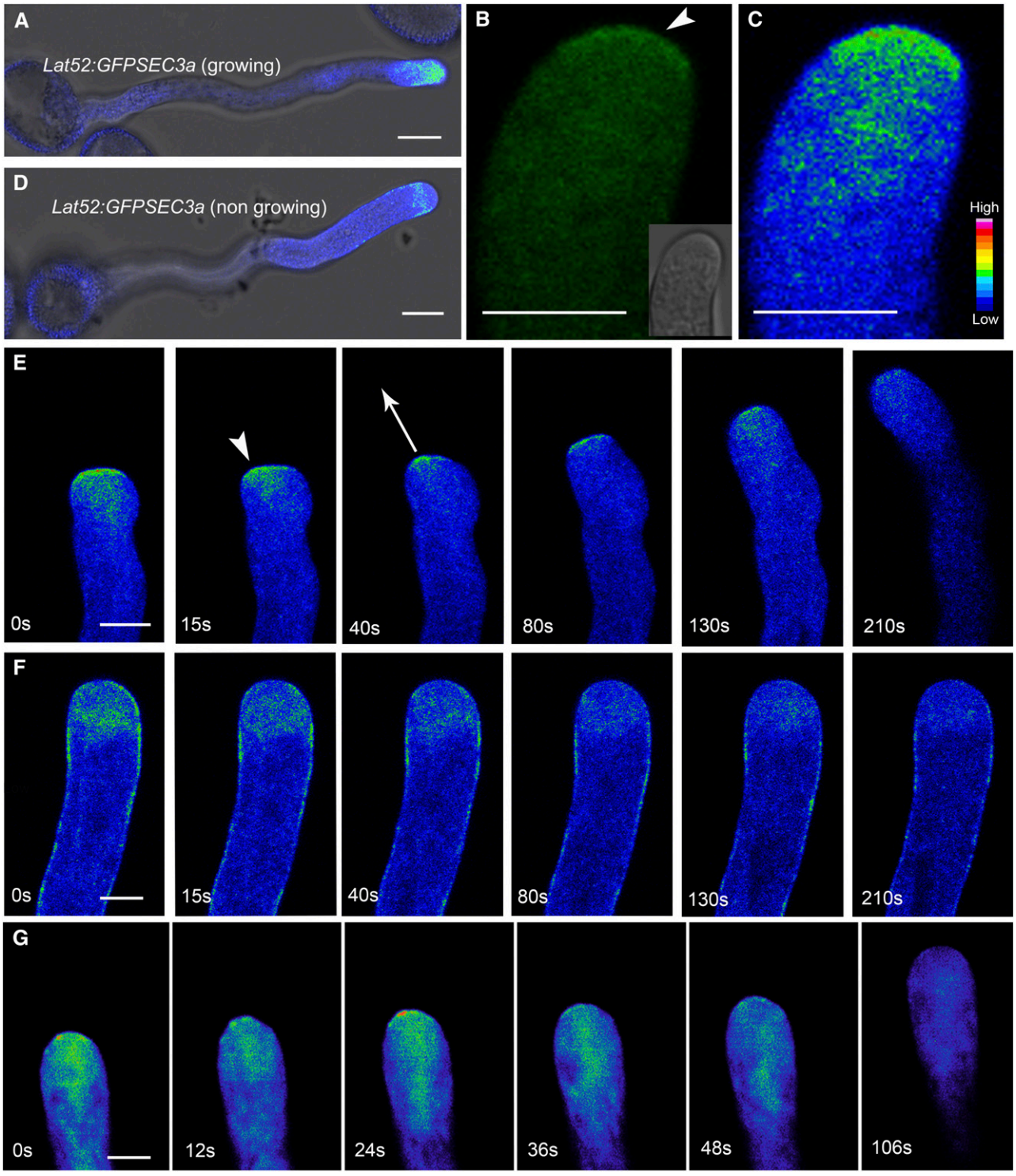

Figure 3. Localization of GFP-SEC3a in growing Arabidopsis pollen tubes. A, In vitro-germinated Arabidopsis pollen stably expressing *LAT52:GFP-SEC3a*. B, Apex of the *LAT52:GFP-SEC3a* pollen tube. The arrowhead marks the membrane localization at the tip. C, The same apex shown in B with GFP signal converted into an intensity scale. D, A nongrowing pollen tube stably expressing *LAT52:GFP-SEC3a*. Note the absence of the protein from the tip. E, Selected time-lapse images showing the localization of GFP-SEC3a in a growing pollen tube. Note that apical localization of GFP-SEC3a is dynamic and the protein accumulates at the future direction of tube growth (arrowhead). The arrow represents the direction of growth as predicted by GFP-SEC3a localization. F, Localization of GFP-SEC3a in a nongrowing pollen tube. The intensity of the GFP signal decreases with time due to high magnification and frequent imaging, and the last frame (210 s) shows the final direction of tube growth after

of pollen tube elongation were detected (Fig. 3E; Supplemental Movies S1 and S2). The frequent frame acquisition used for imaging caused photobleaching of the GFP signal; thus, the last 1.5 min of the time-lapse series highlight primarily the direction of pollen tube elongation. In nonelongating pollen tubes, the GFP-SEC3a signal at the pollen tube apex and tip was reduced (Fig. 3D). Furthermore, no polar accumulation of GFP-SEC3a was detected at the tip, and the signal was distributed evenly on the tube PM apex and flanks (Fig. 3F). Time-lapse imaging revealed that, in nongrowing pollen, the GFP-SEC3a signal on the PM was less dynamic and maintained its location at the flanks (Fig. 3F; Supplemental Movie S3).

To compare these dynamics to those of another exocyst core subunit, we visualized *PSEC8*:*GFP-SEC8* (Fendrych et al., 2010) in Arabidopsis pollen tubes and observed essentially identical localization and dynamics as for SEC3a (Fig. 3G). From these results, we can conclude that pollen tube elongation is characterized by the presence of a mobile polar GFP-SEC3a fraction at the tip that likely marks the sites of exocytic vesicle fusion with the PM and defines the direction of the growth axis.

GFP-SEC3a Tip Accumulation Correlates Directly with the Deposition of PI-Labeled Cell Wall Pectins

To further study the function of SEC3a, we examined its localization relative to PI, which labels esterified pectins in pollen cell walls (Rounds et al., 2014) and has been used previously as a marker for exocytosis in the pollen tube (McKenna et al., 2009). PI was applied to growing pollen at a concentration of 10 μM, and imaging was performed immediately, since under our experimental conditions, pollen tube elongation was inhibited 3 to 5 min after the addition of the dye. In agreement with published data, we observed the strongest PI labeling at the pollen tube tip (Fig. 4A). The GFP-SEC3a signal was observed at the tip PM exactly below the strongest PI staining (Fig. 4B). During pollen tube growth, the pattern of high-PI fluorescence at the tip was maintained, and GFP-SEC3a signal decorated the adjacent plasma membrane (Fig. 4C). We noted that the strongest PI fluorescence at the tip was associated with thicker cell walls at this region compared with the flanks (Fig. 4D), indicating a massive secretion of cell wall material at this location. The direct correlation between PI and GFP-SEC3a signals strongly suggests that the exocyst directs secretory vesicles with essential cell wall components, such as pectins, to the sites of polar exocytosis.

GFP-SEC3a Tip Accumulation Is Correlated Inversely with the PM and Endocytic Vesicle Labeling

Next, we focused on the distribution of GFP-SEC3a compared with recycling/endocytic vesicles. For the visualization of PM and endocytic vesicles, the FM4-64 dye was applied to pollen at a concentration of 1 μM. Under these experimental conditions, FM4-64 did not affect the elongation of pollen tubes (around 4 μm min^{-1} in 13 out of 16 examined pollen tubes), allowing the observation of early stages of FM4-64 labeling. FM4-64 fluorescence reached levels compatible with imaging 3 to 5 min after the addition of the dye. Initially, the staining was detected in the shank and was significantly weaker at the tip PM, while the typical inverted cone of FM4-64-labeled vesicles was not yet observed (Fig. 5A). Importantly, weak tip labeling by FM4-64 was correlated inversely with the accumulation of GFP-SEC3a at the tip and was maintained during pollen tube growth (Fig. 5, B and C). The same pattern of FM4-64 fluorescence was observed following the labeling of wild-type Col-0 nontransgenic pollen tubes (Supplemental Fig. S5), indicating that the low FM4-64 fluorescence at the tip was not due to quenching by GFP-SEC3a. This FM4-64 labeling pattern could be explained by very fast endocytosis at the tip or, more likely, by dilution of the tip membrane by extensive exocytosis, resulting in FM4-64-labeled plasma membrane being pushed away from the tip to the shank. Under our experimental conditions, the typical inverted cone of FM4-64-labeled vesicles was observed 20 to 30 min after application of the dye. However, the distribution of highest FM4-64 and GFP-SEC3A intensities in the inverted cone area was spatially separated (Fig. 5D; compare the intensity range distribution of GFP and FM4-64). The PM at the tip was characterized by a region with low FM4-64 and high GFP-SEC3a signals, both oriented toward the growing direction of the tube, further supporting the extensive exocytosis of de novo-delivered vesicles at this region (Fig. 5, E and F). Importantly, in nongrowing pollen tubes, FM4-64 effectively labeled tip PM (Supplemental Fig. S6). Taken together, these results suggested that the FM4-64-labeled inverted cone consisted mostly of recycling vesicles and was partially separable from the site of exocyst-dependent exocytosis.

Together, the data in Figures 4 and 5 and Supplemental Movies S1 and S2 implicate SEC3a as a bona fide marker for polarized exocytosis in Arabidopsis pollen tubes and suggest that the deposition of cell wall and membrane material is guided by the exocyst complex and is likely partially separable from vesicle recycling at the tip.

Figure 3. (*Continued.*)
3.5 min. Note the cone-shape accumulation of fluorescent signals in growing pollen tubes and their absence in nongrowing tubes. G, Time-lapse images showing the localization of GFP-SEC8 in a growing pollen tube of an in vitro-germinated Arabidopsis pollen, stably expressing *PSEC8*:*GFP-SEC8* in a *sec8-1* mutant background. In A, C, and D to G, GFP fluorescence is represented as an intensity color scale. Bars = 10 μm in A and D and 5 μm in B, C, and E to G.

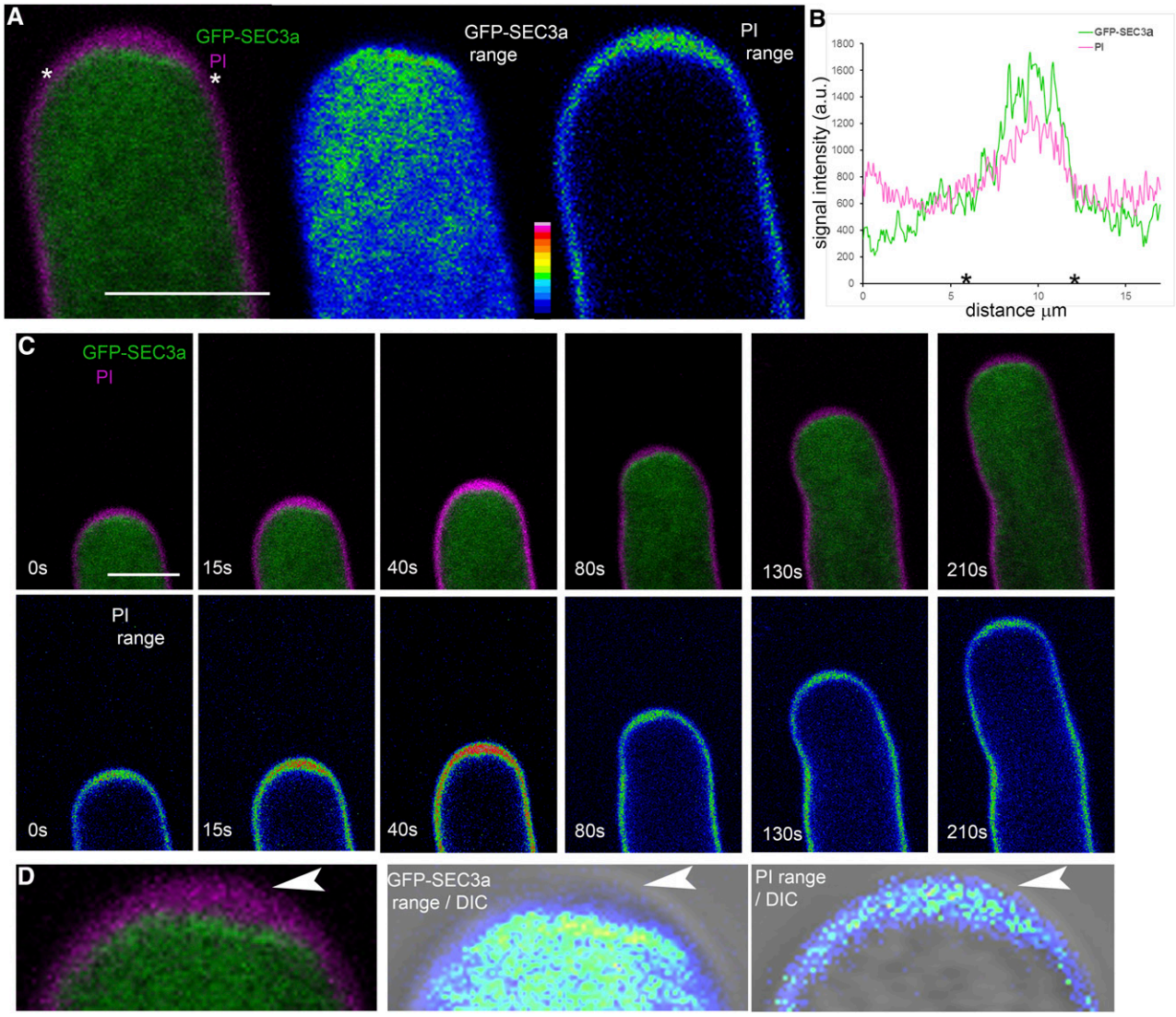

Figure 4. Labeling of GFP-SEC3a Arabidopsis pollen tubes with PI. GFP-SEC3a Arabidopsis pollen tubes were stained with 10 μM PI. A, Apex of a pollen tube showing the localization of GFP-SEC3a and PI with intensity scale for each channel. Asterisks mark positions on the intensity plot in B. B, Intensity plot of GFP and PI signals across the plasma membrane/cell wall of pollen apex (including flanks). Asterisks mark positions on the corresponding image in A. C, Time-lapse images of a growing pollen tube. Note that GFP-SEC3a decorates the PM beneath the strongest PI signal at the tip. D, Enlarged images of the pollen tip showing thick cell wall at the tip (arrowheads) and GFP-SEC3a signal decorating the PM at this region. a.u., Arbitrary units. Bars = 5 μm.

Partially Complemented *sec3a-1* Pollen Develop Multiple Tips

To further study the function and localization of SEC3a in pollen development, we examined the phenotype of *sec3a-1* mutant pollen complemented with GFP-SEC3a (Fig. 6). As expected from the self-crosses and reciprocal crosses displaying complementation of the male transmission of *sec3a-1* (Table I; Supplemental Tables S1 and S2), normal-looking pollen tubes were observed in which GFP-SEC3 was localized at the tip (Fig. 6, A and B). However, the growth rate of the *sec3a-1;GFP-SEC3a* pollen tubes was around 1.5 μm min^{-1} (n = 7) compared with 3.5 to 4 μm min^{-1} for wild-type Col-0/*GFP-SEC3a* pollen tubes. Interestingly, in some pollen grains, multiple tips germinated from more than one germination pore, indicating that SEC3a is required to determine the pollen tube germination site. Similar to its distribution in wild-type Col-0, in elongating *sec3a-1* pollen tubes, GFP-SEC3a accumulated at the apical tip and was spatially separable from FM4-64-labeled PM (Fig. 6, C and D).

In the multiple-tip *sec3a-1/GFP-SEC3a* complemented pollen, one pollen tube continues growing while the other(s) arrests. Likely, the overexpression of GFP-SEC3 is able to induce multiple germination pore activation but is unable to maintain the multiple tip growth,

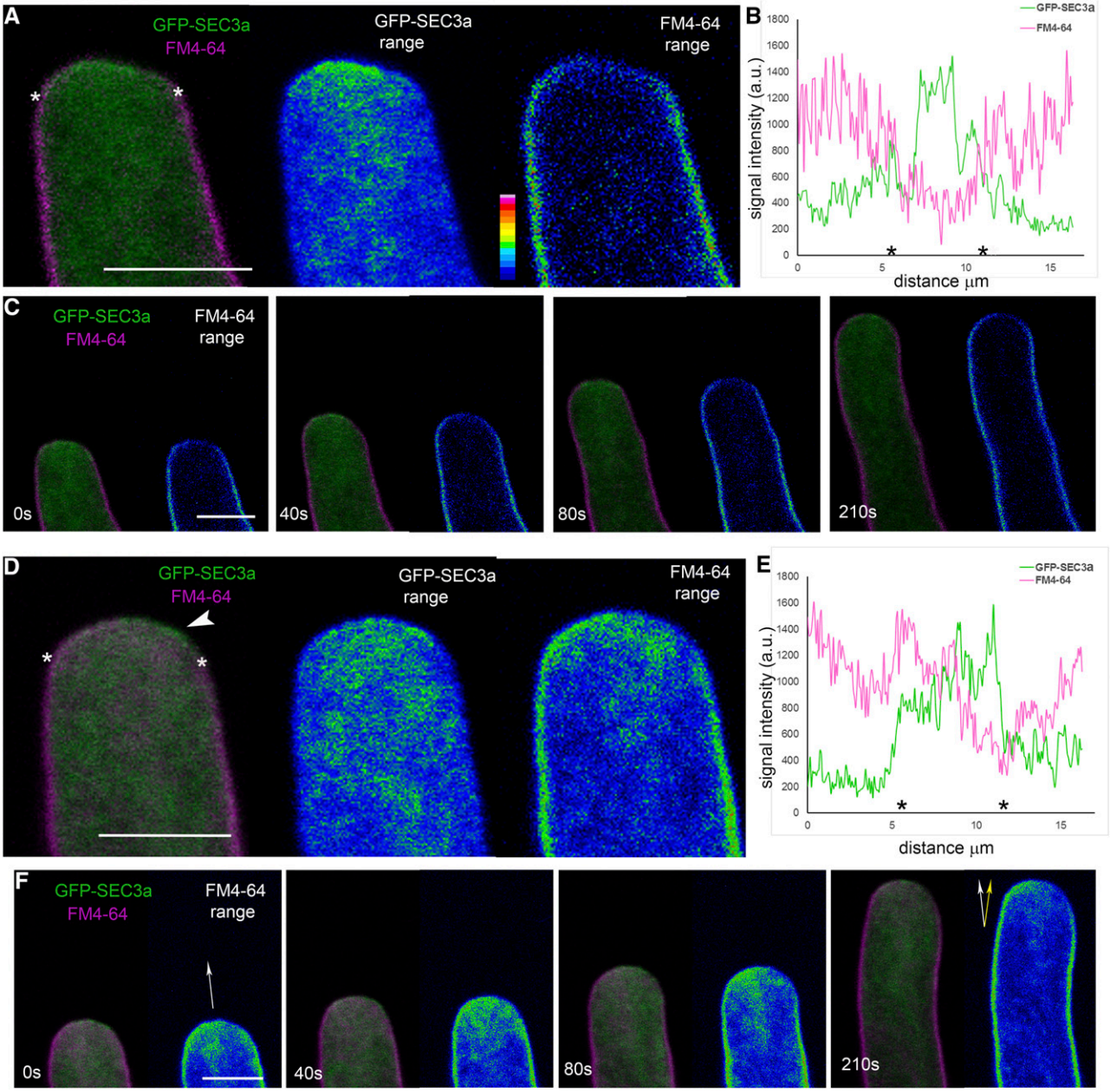

Figure 5. Labeling of GFP-SEC3a Arabidopsis pollen tubes with FM4-64. GFP-SEC3a Arabidopsis pollen tubes were labeled with 1 μM FM4-64 for 3 min (A–C) or 20 min (D–F) and then subjected to imaging. A and D, Apex of the pollen tube showing the localization of GFP-SEC3a and FM4-64 with intensity scale for each channel. Asterisks mark positions on the intensity plots in B and E. The arrowhead in D points to the region with high GFP-SEC3a and low FM4-64 signals. B and E, Intensity plots of GFP and FM4-64 signal across the PM of the pollen apex (including flanks). Asterisks mark positions on the corresponding images in A and D. C and F, Time-lapse images showing the localization of GFP-SEC3a and FM4-64 in growing pollen tubes. In F, the white arrows mark the direction of pollen tube elongation as predicted from tip geometry, and the yellow arrow indicates the actual growth direction. Note that the position of high GFP and low FM4-64 signals correlates with growth direction. a.u., Arbitrary units. Bars = 5 μm.

resulting in only one growing tip. This feature allowed us to further characterize the function of SEC3a in pollen tube growth and correlate it with the secretion of esterified pectins. LM19 and LM20 are monoclonal antibodies that recognize deesterified and methyl-esterified homogalacturonans (pectins), respectively (Verhertbruggen et al., 2009). In wild-type Col-0, LM19-labeled deesterified pectins were detected from the early stages of pollen germination at the emerging bud and in elongated pollen tubes at the tip and along the shank (Fig. 6E). In *sec3a-1/GFP-SEC3* multiple-tip pollen, deesterified pectins were observed both in the

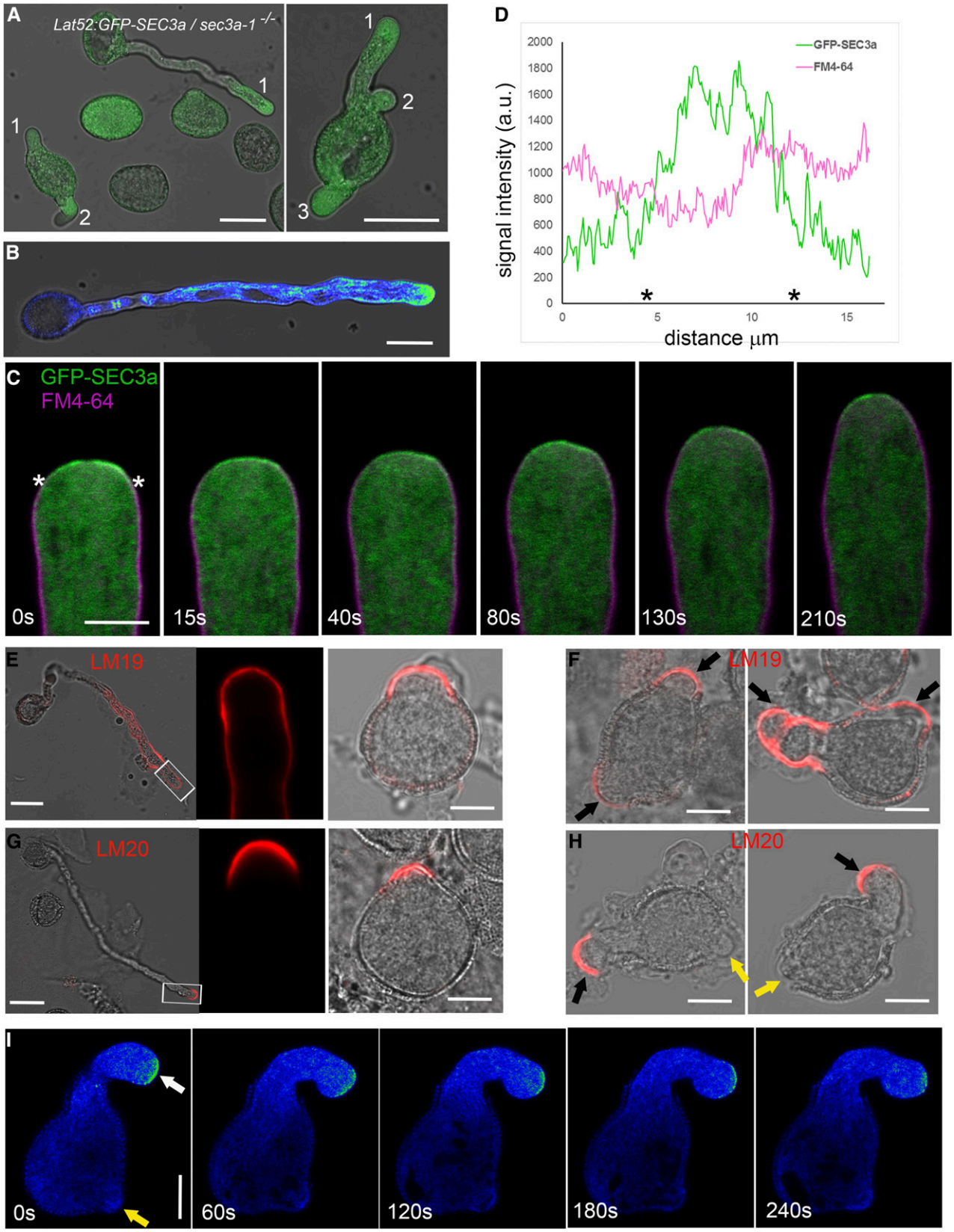

Figure 6. Expression of GFP-SEC3a in the *sec3a-1* homozygous background results in the development of pollen with multiple tips. A, Germinating *sec3a-1* pollen expressing *GFP-SEC3a*. The multiple tips are marked by numbers. B, In pollen tubes with one

growing and in the arrested tubes (Fig. 6F). In agreement with published results on tobacco and Arabidopsis pollen tubes (Chebli et al., 2012; Leroux et al., 2015), the LM20-labeled esterified pectins were observed only at the tip of elongating pollen tubes and at the bud of germinating pollen, where they are secreted (Fig. 6G). Significantly, in *sec3a-1/GFP-SEC3a* pollen, the esterified pectins were observed only at the tip of the growing pollen tubes but not in the arrested pollen tubes (Fig. 6H). Taken together, the results in Figure 6, F and H, indicated that esterified pectins are actively secreted only in the growing tube of *sec3a-1/GFP-SEC3a*, while the arrested tube only contains pectins that have been deesterified.

Unfortunately, GFP-SEC3a signal at the tip PM was lost following the fixation and labeling of cell wall epitopes; in addition, the protocol is not compatible with antibody labeling of intracellular proteins. As an alternative, we examined the localization of GFP-SEC3a at the growing and arrested pollen tubes at high resolution. In all pollen that were examined (n = 10), the typical GFP-SEC3a tip-focused PM fraction was detected only at the tip of the growing tube, while no tip-focused PM fraction was detected in the arrested pollen tubes (Fig. 6I; Supplemental Movies S4 and S5). These data indicated that there is strong positive correlation between the localization of GFP-SEC3a at the tip of growing pollen tubes and the secretion of esterified pectins and further established GFP-SEC3a as an intracellular marker for exocytosis.

Plasma Membrane Localization of SEC3a in Tobacco Pollen Tube Requires an Intact N-Terminal PH Domain

The transient expression of fluorescent proteins in tobacco pollen tubes is a commonly used model system for studying the localization of polarity determinants, due to the larger diameter and well-defined zonation of the pollen tube apex compared with Arabidopsis. *LAT52:YFP-SEC3a* and *LAT52:SEC3a-YFP* fusion proteins were transiently expressed in tobacco pollen tubes. Interestingly, the distribution of SEC3a in tobacco pollen partially differed from that observed in Arabidopsis and depended on the mode of cell elongation. In pollen tubes showing steady nonoscillatory growth, both YFP-SEC3a and SEC3a-YFP showed cytoplasmic localization with enhanced fluorescence at the PM in the subapical region, with maximum signal located 2 to 7 μm behind the apex (Fig. 7A; Supplemental Fig. S7). It is unlikely that this localization was due to the heterologous nature of Arabidopsis SEC3a in tobacco pollen, since the tobacco SEC3a homolog localized to the same region (Supplemental Fig. S7). During steady growth, the localization of the full-length SEC3a remained essentially subapical, although some periodic changes in signal intensity could be observed (Fig. 7, B and D). In contrast, the localization of SEC3a in oscillating tobacco pollen tubes also showed an oscillatory behavior, alternating between cytoplasm and apical plasma membrane (Fig. 7, A and C). Kymograph analysis suggested that a period of fast elongation was associated with the accumulation of SEC3a in the cell apex, which was followed by a temporal growth arrest and concomitant dissociation of SEC3a from the membrane (Fig. 7E). In nongrowing tobacco pollen tubes, SEC3a was distributed evenly along the apex and subapical regions (Supplemental Fig. S7).

It has been demonstrated that the N-terminal domain of the yeast Sec3p, consisting of amino acids 1 to 320, interacts with PIP_2 (Zhang et al., 2008). Additional studies showed that the 75 to 248 domain of yeast Sec3p folds into a PIP_2-binding PH domain (Baek et al., 2010; Yamashita et al., 2010). To get an evolutionary insight into SEC3 function, we identified SEC3 homologs in diverse eukaryotic species. Although the general sequence identity between SEC3 homologs is rather low, we found that most of them contain a region corresponding to the PH domain. Calculation of the phylogenetic relationship between SEC3 amino acid sequences, based on either the SEC3 domain or the PH domain, showed that the distribution of SEC3 mostly follows organismal evolution (Supplemental Fig. S8). Supplemental Figure S9 shows an alignment of N-terminal regions corresponding to the PH domain of selected SEC3 proteins. We then fused the N-terminal 180-amino acid domain of Sec3a (SEC3a-N; the region corresponding to the yeast PH domain) to YFP and used it for transient expression in tobacco pollen tubes. YFP-SEC3a-N exhibited the same subapical localization pattern that was observed for the full-length protein in steady-state growing cells (Fig. 7, F and G). Interestingly, YFP-SEC3a-N and SEC3a-N-YFP showed an even stronger association with the plasma membrane

Figure 6. (*Continued.*)
tip, *GFP-SEC3a* concentrates at the apex (GFP fluorescence is shown as an intensity color scale). C, Selected time-lapse images of *sec3a-1*/GFP-SEC3a pollen labeled with 1 μM FM4-64 for 20 min. Note that GFP-SECa effectively accumulates at the apical plasma membrane. D, Intensity plot of GFP and FM4-64 signal across the PM of pollen apex (including flanks). Asterisks mark positions on the corresponding image in C. E to H, Immunolabeling of deesterified pectins (E and F) and esterified pectins (G and H) with LM19 and LM20 monoclonal antibodies, respectively. E and G, Nontransgenic Col-0 pollen. F and H, *sec3a-1/GFP-SEC3a* pollen. The white rectangles in E and G highlight the enlarged regions shown in the middle image of each panel. The black arrows highlight germinated pollen tubes in F and the actively growing pollen tubes in H. The yellow arrows in H highlight the arrested small pollen tubes. I, Localization of GFP-SEC3a in multiple-tip *sec3a-1/GFP-SEC3a* pollen. The white arrow denotes the growing pollen tube, and the yellow arrow indicates the arrested pollen tube. See also Supplemental Movies S4 and S5. a.u., Arbitrary units. Bars = 20 μm in A, B, E, and G, 10 μm in F, H, and I, and 5 μm in C.

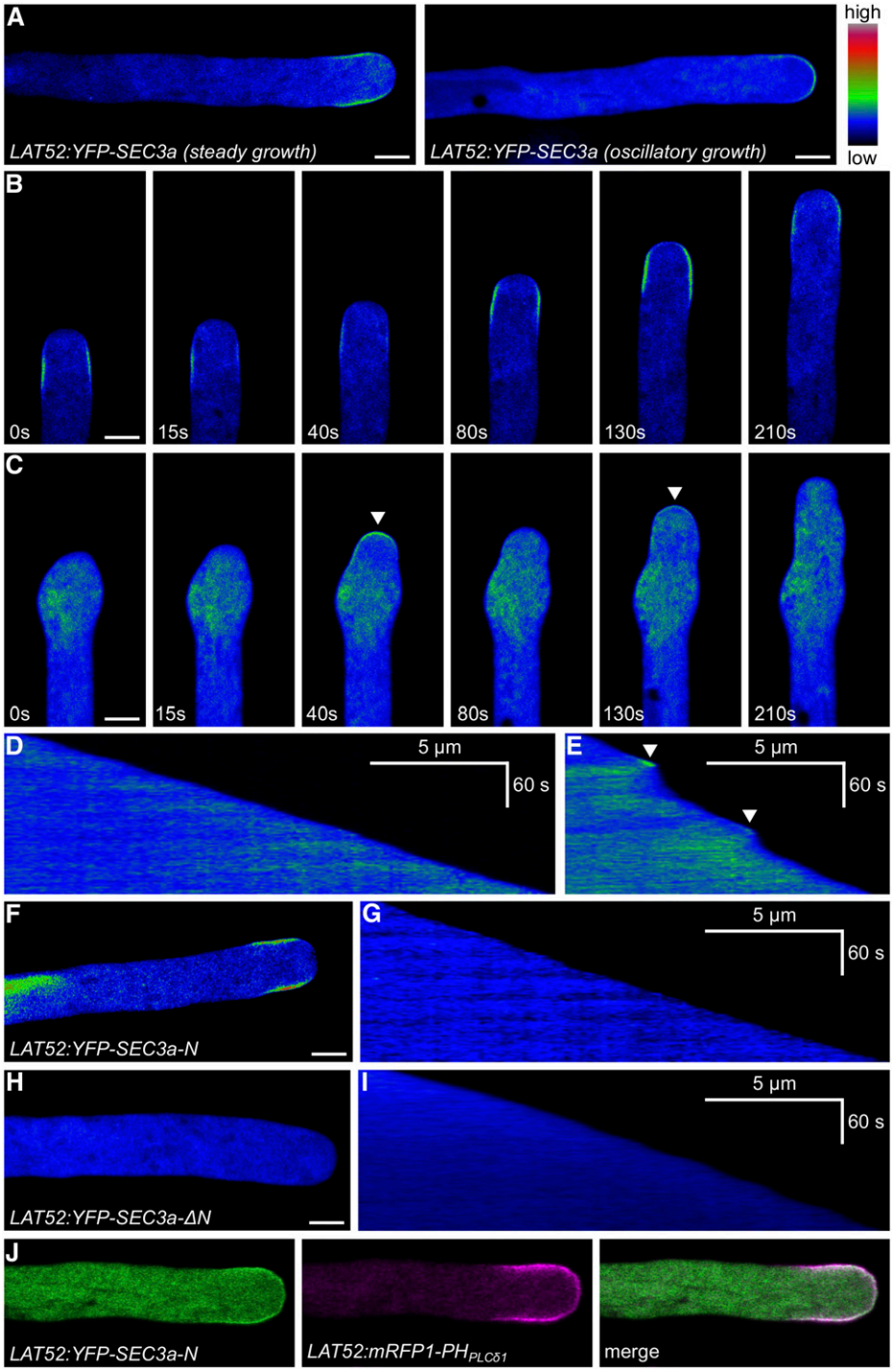

Figure 7. The N-terminal PH domain of Arabidopsis SEC3a colocalizes with PIP_2 and is responsible for the localization of SEC3a at the plasma membrane in tobacco pollen tubes. A, Localization of full-length YFP-SEC3a transiently expressed in tobacco pollen tubes under the control of the *LAT52* promoter. B and C, Selected time-lapse images showing the localization of *LAT52:YFP-SEC3a* in steady-growing (B) and oscillating (C) pollen tubes. D and E, Kymograph analysis of growth and apical YFP-SEC3a fluorescence in steady-growing (D) and oscillating (E) pollen tubes. Arrowheads in C and E point to dynamic apical localization of SEC3a in oscillating pollen tubes. F and G, Localization (F) and kymograph analysis (G) of the SEC3a N-terminal domain (*LAT52:YFP-SEC3a-N*). H and I, Localization (H) and kymograph analysis (I) of SEC3a lacking its N-terminal domain (*LAT52:YFP-SEC3a-ΔN*). J, Colocalization of YFP-SEC3a-N with the PIP_2 marker mRFP1-$PH_{PLC\delta1}$. In A to I, YFP fluorescence is represented as an intensity color scale. PLC, Phospholipase C. Bars = 5 μm.

than the full-length protein (Fig. 7F; Supplemental Fig. S7).

Since the canonical role of PH domains is the interaction with membrane phosphatidylphosphoinositides (PPIs), we next tested whether SEC3a-N localization corresponds to the distribution of PIP_2 in the PM. The PIP_2 marker mRFP1-$PH_{PLC\delta1}$ (Helling et al., 2006) localized to the PM with enhanced fluorescence at the subapical region of the pollen tube apex. YFP-SEC3a-N colocalized with mRFP1-$PH_{PLC\delta1}$ at the pollen tube apex, suggesting that its localization involves an association with PIP_2 (Fig. 7J). This experiment suggested that the N-terminal part of SEC3a is able to bind signaling phospholipids. Interestingly, the overexpression of full-length SEC3a or SEC3a-N in pollen tubes caused a marked reduction of growth rate, induced the swelling of pollen tube tips, and was associated with a nondynamic distribution of fluorescence along the

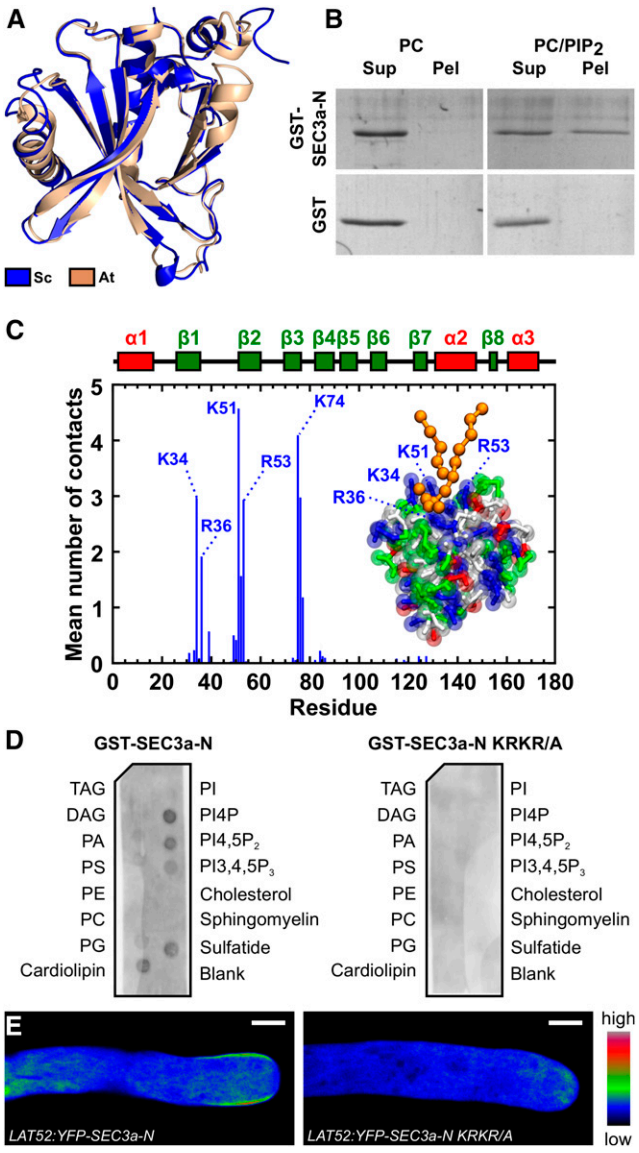

Figure 8. SEC3a-N binds phosphoinositides via four positively charged residues that mediate its association with the plasma membrane in tobacco pollen tubes. A, Comparison of the final relaxed SEC3a-N homology model (At) with the yeast template structure (Sc). B, Liposome-binding assay of GST-SEC3a-N. PIP_2 binding was determined using 200-nm vesicles containing 5% PIP_2:95% PC or PC alone. After incubation of GST-SEC3a-N with the vesicles, they were recovered by ultracentrifugation, and protein bound (Pel) was analyzed by SDS-PAGE. As a negative control, GST alone was used. Representative results from three independent experiments are shown. Sup, Supernatant. C, Analysis of MD simulations displaying polar contacts of SEC3a-N with a PIP_2 molecule. The bars represent average numbers of polar contacts through the last 8 μs of the simulation. Polar contacts were defined as the number of PIP_2 head group atoms within 8 Å of protein atoms. The inset image represents a coarse-grained model of SEC3a-N coordinating the PIP_2 molecule. The interacting residues are highlighted. D, Lipid-binding properties of wild-type GST-SEC3a-N and mutated GST-SEC3a-N KRKR/A recombinant proteins, as determined using a protein-lipid overlay assay. DAG, Diacylglycerol; PA, phosphatidic acid; PE, phosphatidylethanolamine; PG, phosphatidylglycerol; PI4P, phosphatidylinositol 4-phosphate; $PI4,5P_2$, phosphatidylinositol 4,5-bisphosphate; $PI3,4,5P_3$, phosphatidylinositol 3,4,5-trisphosphate; PS, phosphatidylserine; TAG, triacylglycerol. E, Localization of wild-type YFP-SEC3a-N and the mutated variant YFP-SEC3a-N KRKR/A in tobacco pollen tubes. YFP fluorescence is represented as an intensity color scale. Bars = 5 μm.

pollen tube tip and shank (Supplemental Fig. S7), similar to nongrowing tobacco and Arabidopsis tubes. To further examine whether the SEC3a N-terminal domain is involved in membrane localization, we transformed tobacco pollen tubes with truncated SEC3a lacking the N terminus (i.e. region 181–887; SEC3a-ΔN). In agreement with the colocalization of SEC3a-N with $PH_{PLC\delta1}$, both YFP-SEC3a-ΔN and SEC3a-ΔN-YFP localized only to the cytoplasm (Fig. 7, H and I; Supplemental Fig. S7).

The Combination of Biochemical Approaches and Structural Modeling Reveal That SEC3a-N Specifically Binds Membrane Phosphoinositides

Given the fact that, despite their low sequence identity, PH domains form a similar fold with a core consisting of seven antiparallel β-strands capped by a terminal α-helix (Lemmon, 2008), we modeled a structure of Arabidopsis SEC3a-N using the template-based approach with crystalized yeast Sec3p-N (3A58; Yamashita et al., 2010) as a template. The resulting model was energetically relaxed by short all-atom molecular dynamics (MD) simulation (30 ns). The final model of SEC3a-N (Fig. 8A) had a ProSA score of −4.92 (Wiederstein and Sippl, 2007), which is comparable to the template score (−5.43), thus implying that, despite the low primary sequence identity, our computed model is valid.

To confirm that SEC3a-N directly binds PIP_2, we fused it to glutathione *S*-transferase (GST-SEC3a-N) and expressed it in *Escherichia coli*. The purified recombinant GST-SEC3a-N was used in two widely applied in vitro lipid-binding experiments: the large unilamellar vesicle cosedimentation assay and the protein-lipid overlay assay. In large unilamellar vesicle cosedimentation assays, GST-SEC3a-N bound to large unilamellar vesicles containing 5% PIP_2 in phosphatidylcholine (PC) but not to vesicles containing only PC (Fig. 8B). In agreement, GST-SEC3a-N bound several PPIs, including PIP_2, in protein-lipid overlay assays (Fig. 8D).

To further test the binding modes of PIP_2 by SEC3a-N, we used coarse-grained MD with the MARTINI force field (Marrink et al., 2007; Monticelli et al., 2008) and simulated the self-assembly of a lipid bilayer in the presence of the modeled structure of the SEC3a-N domain, as this approach was shown to be advantageous for the characterization of peripheral membrane protein dynamics (Pleskot et al., 2012). The simulation box contained the SEC3a PH domain, 256 lipids, water, and ions. In total, we performed 16-μs-long simulations

for each system. We observed that, in simulations with one PIP_2 molecule in the PC bilayer, the Arabidopsis SEC3a PH domain was targeted rapidly to the membrane and remained bound to PIP_2, showing that the system was in equilibrium. In contrast, in a system with a PC-only membrane, SEC3a-N was never bound to the bilayer and remained in the virtual cytoplasm. Analysis of amino acid residues interacting with the PIP_2 molecule, as revealed by the coarse-grained MD simulation, showed that the PIP_2 molecule was coordinated by several positively charged amino acid residues located between loops $\beta1/\beta2$ and $\beta3/\beta4$, namely Lys-34, Arg-36, Lys-51, Arg-53, and Lys-74 (Fig. 8C).

To test the importance of positively charged residues for PIP_2 binding, we generated a mutated GST-SEC3a-N, where the residues with the greatest number of polar contacts with the PIP_2 molecule, namely Lys-34, Arg-36, Lys-51, and Arg-53 (Fig. 8C), were changed to Ala. The resulting GST-SEC3a-N KRKR/A mutant did not interact with PIPs in vitro (Fig. 8D). Moreover, the YFP-SEC3a-N KRKR/A mutant completely lost the ability to bind the plasma membrane following transient expression in tobacco pollen tubes (Fig. 8E). Interestingly, the overexpression of mutated YFP-SEC3a-N never induced the depolarization of the pollen tube tip caused by wild-type YFP-SEC3a-N (Supplemental Fig. S7). These results indicated that the N-terminal region of SEC3a contains a functional PIP_2-binding domain capable of interaction with the PM and suggested that binding to PIP_2 might have an important role in subapical shank localization of SEC3a.

The N-Terminal PH Domain Is Not Essential for SEC3a Function and Localization in Arabidopsis Pollen

Next we employed genetic analysis to examine the importance of the N-terminal PH domain for SEC3a function. To this end, we complemented the *sec3a-1* mutant with *LAT52:SEC3a-ΔN*, which lacks the first 180 amino acids, and with *LAT52:SEC3a KRKR/A*. Successful complementation of male transmission defects associated with the *sec3a-1* allele was observed in several independent lines expressing *LAT52:SEC3a-ΔN*, *LAT52:GFP-SEC3a-ΔN*, *LAT52:SEC3a KRKR/A*, and *LAT52:GFP-SEC3a KRKR/A* (Supplemental Table S4). The ability of *SEC3a-ΔN*, *GFP-SEC3a-ΔN*, *SEC3a KRKR/A*, and *GFP-SEC3a KRKR/A* to complement the male transmission defect of the *sec3a-1*$^{+/-}$ mutant indicates that the SEC3a N-terminal domain and a functional PH domain are not absolutely required for SEC3a function in Arabidopsis. To address whether the PM association of the N-terminal SEC3a mutants was affected, we analyzed the localization of GFP-SEC3a KRKR/A and GFP-SEC3a-ΔN stably expressed in Arabidopsis transgenic pollen tubes. Both mutants exhibited enrichment of the GFP signal at the pollen tube apex similar to GFP-SEC3a (Fig. 9, A–C). Moreover, time-lapse imaging revealed that, similar to wild-type GFP-SEC3a, the GFP-SEC3a KRKR/A and GFP-SEC3a-ΔN mutants are highly dynamic and decorate the PM at the pollen tube tip (Fig. 9D; Supplemental Movies S6–S9). Hence, the localization and function of SEC3a in Arabidopsis pollen tubes can take place independently of PIP_2 binding.

DISCUSSION

SEC3a Is Essential for Exocyst Function in Pollen Tube Germination Growth

A plant SEC3 mutant was first identified in maize and designated *rth1* based on the compromised root hair elongation (Wen and Schnable, 1994; Wen et al., 2005). Interestingly, the maize *rth1* mutant also displays dwarf stature and does not produce seeds. While cereals feature two distinct SEC3 subclasses, Arabidopsis and other dicot plants harbor a single class of SEC3 subunits, which duplicated independently in most known cases (Supplemental Fig. S8; Cvrčková et al., 2012). Here, we show that, in Arabidopsis, the loss of only one of these duplicated paralogs, *SEC3a*, results in a complete male gametophyte transmission defect, as was shown previously for *sec8*, *sec6*, *sec15a*, and *sec5a/sec5b* single and double mutants (Cole et al., 2005; Hála et al., 2008). The T-DNA insert in *sec3a-1* is mapped to the last exon, 52 bp upstream of the stop codon. The absence of endogenous *SEC3a* mRNA in *sec3a-1*$^{-/-}$*/LAT52:SEC3a* plants indicates that *sec3a-1* is a null allele. In the Arabidopsis genome, gene duplications often are associated with divergences in the expression pattern of the paralogs and are indicative of regulatory subfunctionalization or neofunctionalization (Liu et al., 2011), which might be the case for *SEC3a* and *SEC3b*. The low expression levels of *SEC3b* in germinating pollen and the lack of an obvious phenotype in *sec3b-1* homozygotes, together with the compromised pollen tube growth of *sec3a-1* plants, indicate that *SEC3a* is the main paralog responsible for SEC3 function in Arabidopsis pollen germination and growth.

An Arabidopsis *SEC3a* loss-of-function mutant, carrying a SALK T-DNA insertion in the first intron of the *SEC3a* paralog, was shown to display developmental abnormalities resulting in embryonic lethality but no pollen tube growth defects (Zhang et al., 2013). We have examined the same SALK T-DNA line (SALK_145185) described by Zhang et al. (2013) using PCR and sequencing and were unable to detect a T-DNA insert in the *SEC3a* gene. According to our sequencing analysis, the *SEC3a* gene is intact in the SALK_145185 line. Unfortunately, only primers for amplifying the cDNAs of exocyst subunits were described in Supplemental Table S1 in the article by Zhang et al. (2013), and a description of the primers used for genotyping of the SALK_145185 line is missing. The primers listed for *SEC3a* are not specific and would amplify *SEC3b* as well. Furthermore, the first intron of *SEC3a* contains a tandem repeat; as a result, the flanking sequence reported for SALK_145185 is partially similar to two other regions in the *SEC3a* first intron. Therefore, it appears that the

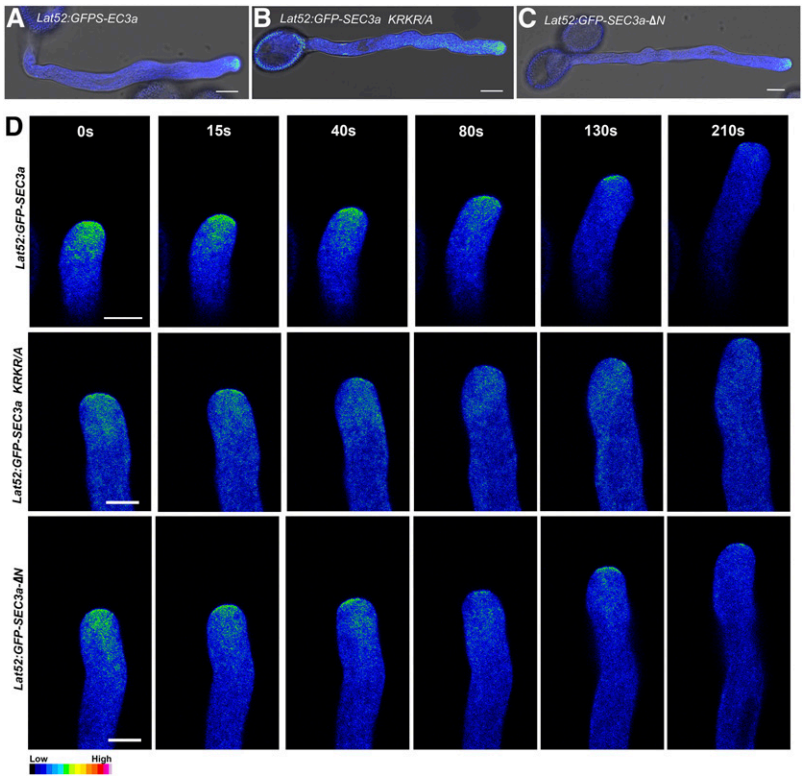

Figure 9. The N-terminal PH domain of SEC3a is not required for its accumulation at the tip of growing Arabidopsis pollen tubes. A to C, In vitro-germinated Arabidopsis pollen tubes stably expressing GFP-SEC3a (A) GFP-SEC3a KRKR/A (B), and GFP-SEC3-ΔN (C) under the regulation of the *LAT52* promoter. D, Selected time-lapse images of growing GFP-SEC3a, GFP-SEC3a KRKR/A, and GFP-SEC3a-ΔN Arabidopsis pollen tubes. GFP fluorescence is represented as an intensity color scale. Bars = 10 μm in A to C and 5 μm in D.

information on the genotyping of SALK_145185 provided by Zhang et al. (2013) is insufficient.

We have characterized a different allele of *sec3a* from a different mutant collection (GABI-KAT). Based on our genetic, molecular, and phenotypic analyses, the complementation of the male transmission and pollen tube growth defects by either SEC3a or GFP-SEC3a, and the similarity to other exocyst subunit mutants, it is unclear how the male transmission defect in *sec3a-1* could be overcome to result in a homozygous sporophytic null mutant. Loss-of-function mutants in different exocyst subunits (except subunits with a large number of homologs, like EXO70) produce the same pollen transmission defects, implicating the exocyst complex in pollen germination and pollen tube growth. Our data also rule out a redundant function of *SEC3b* (Supplemental Fig. S3).

Interestingly, mutations in all exocyst subunits tested to date (Cole et al., 2005; Hála et al., 2008), including the *sec3a-1* mutant, are not associated with transmission defects through the female gametophyte, suggesting that the exocyst is not essential for its development or that the sporophytic exocyst survives through female meiosis and megaspore development. Similar to the severe *sec8* mutant alleles, *sec3a-1* has absolute male transmission defects, while the early stages of pollen development are not affected by the mutations (Cole et al., 2005). Tetrad analysis of several exocyst mutants, including *sec8*, showed that short, aberrant pollen tubes are formed at low frequencies in vitro (Hála et al., 2008). Interestingly, in *sec3a-1* tetrads, the frequencies of germinated pollen, both in vitro and in vivo, were significantly lower, indicating an interesting difference in the requirement of exocyst subunits in early pollen grain activation/germination and growth. Similar differential functions of exocyst subunits also are known in yeast (Wiederkehr et al., 2004) and in the fruit fly (Jafar-Nejad et al., 2005; Mehta et al., 2005).

Polar Localization of SEC3a in Arabidopsis and Tobacco Pollen Tubes

The apex of a growing pollen tube is characterized by the presence of numerous vesicles that form an inverted cone-shaped structure beneath the apical PM and deliver essential cell wall and membrane components to the growing tip (Hepler and Winship, 2015). Localization of GFP-SEC3a to the tip PM in Arabidopsis pollen tubes suggests its function as a landmark for secretory vesicles and supports its role in polarized exocytosis. In agreement, immunolocalization studies with fixed pollen tubes showed SEC6, SEC8, and EXO70A1 signal maxima at the membrane and in the tip inverted cone area (Hála et al., 2008). Similar distributions were observed for other proteins in the pollen tube, including the putative exocyst regulators Rab and ROP GTPases (Cheung and Wu, 2008; Guan et al., 2013). In this respect, our observations and conclusions also are different from the conclusions recently published by Zhang et al. (2013), who stated that SEC3a is not involved in polarized secretion in root hairs. As pollen

tubes elongate at an extremely fast rate, it is obvious that the delivery of exocytotic vesicles to the tip must be not only focused and efficient but also flexible, to allow fluctuations in the direction of the growth axis during elongation. A dynamic and tip-focused localization of GFP-SEC3a with a maximum that predicts the direction of tube elongation is thus in agreement with the proposed role of SEC3a as a landmark for polarized exocytosis (Fig. 10A). Our analysis of nonelongating pollen tubes suggests that a focused and dynamic, rather than a stable, association of SEC3a with the PM is essential for effective elongation of the pollen tube apex. The dynamic localization of SEC3a puncta and their transient association with the tip PM are similar to those of other exocyst subunits at the lateral domain of root epidermis visualized by variable-angle epifluorescence microscopy (Fendrych et al., 2010).

It was shown previously that exocytosis and cell wall thickening oscillate and precede the increase in growth rate in oscillating pollen tubes (McKenna et al., 2009). Because pectins make up the bulk of the secreted material at the pollen tube tip, the correlation between the localization of high-PI signal at the tip, the localized labeling of esterified pectins by the LM20 monoclonal antibodies, and the decoration of the PM by GFP-SEC3a suggests that the exocyst is involved in the polarized secretion of cell wall pectins (Fig. 10A). The analysis of the multiple-tip *sec3a-1/GFP-SEC3a* complemented pollen revealed that GFP-SEC3a is localized at the tip PM and that esterified pectins are secreted only in the growing but not in the arrested tubes. Studies in lily (*Lilium longiflorum*), tobacco, and Arabidopsis pollen tubes demonstrated the importance of pectin deesterification and the resultant cross-linking in pollen tube morphogenesis and tip growth. Pectins are secreted at the tip together with PME. In turn, PME deesterifies the pectins, leading to cross-linking of the pectin homogalacturonan chains by Ca^{2+} at the shank. The cross-linking of the pectin chains leads to cell wall stiffening at the shank while leaving the cell wall at the tip softer, thereby yielding more to intracellular turgor (McKenna et al., 2009; Chebli et al., 2012). While this mechanism is believed to be essential for tip growth, it is not known whether the differential composition of the cell wall at the tip and the shank affects the exocytotic machinery.

The compromised male transmission and the complete inhibition of pollen tube germination in exocyst subunit mutants have hampered the analysis of exocyst function. The partial complementation of *sec3a* pollen tube germination by GFP-SEC3a has enabled us to

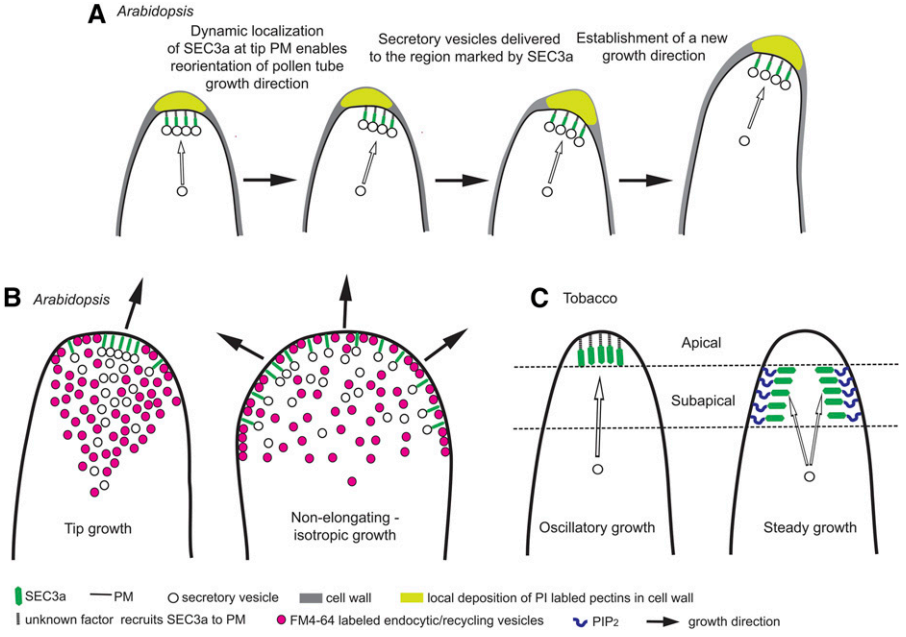

Figure 10. SEC3a function and localization in pollen tube tip growth. A, SEC3a localization at the tip PM is dynamic and defines the direction of pollen tube growth. Secretory vesicles, presumably loaded with pectins, are delivered to the region on the tip PM marked by SEC3a, resulting in the local deposition of pectins. B, In elongating pollen tubes, the PM at the tip is characterized by a region with high GFP-SEC3a and low FM4-64 signals, which could be considered a polar domain of focused and extensive exocytosis. In nonelongating pollen tubes, GFP-SEC3 signal on the PM is homogenously distributed across the tip and shank PM. As a consequence, a polar domain for exocytosis is not established and the tubes grow isotropically. C, In tobacco, SEC3a PM localization depends on the mode of pollen tube growth. During steady growth, SEC3a localizes to a subapical region and requires PIP_2 for the association with membrane. In oscillatory growing pollen tubes, SEC3a association with the PM at the tip is dynamic, as in Arabidopsis. The difference in SEC3a localization between these two growing modes likely reflects the actual site for the delivery of secretory vesicles.

study exocyst function during pollen tube development and growth. The development of pollen with multiple tips (Fig. 6A) in *sec3a/GFP-SEC3a* mutant pollen indicated that SEC3a is required for the determination and activation of the pollen tube germination pore and/or maintenance of the germination site and further tip growth. The function of SEC3a in determining the site of the germination pore is in agreement with the earlier manifestation of the *sec3a-1* mutant defect in pollen germination, as compared with other exocyst mutants. Similar to *sec3a-1/GFP-SEC3a*, *pme48* mutant pollen developed multiple tips, indicating that pectin deesterification is required for the selection/maintenance of a single germinating tip (Leroux et al., 2015). In *pme48*, the LM20-labeled esterified pectins were more abundant and less focally localized (Leroux et al., 2015). In contrast, in *sec3a-1/GFP-SEC3a* pollen, the LM20-labeled esterified pectins were highly focused at the tip of the growing pollen tube and absent from the arrested tube. Therefore, it is likely that the mechanisms responsible for the formation of multiple tips are different in the two mutants. Leroux et al. (2015) suggested that, in *pme48*, multiple tips emerged due to the softening of the cell wall that contained higher levels of esterified pectins. It is likely that multiple tips in *sec3a-1/GFP SEC3a* resulted from the ectopic activity of GFP-SEC3a that, in some cases, supported bud site selection/initiation but failed to maintain tube growth.

The simultaneous visualization of FM4-64 labeling and GFP-SEC3a allowed us to separate between the tip growth domain, where the exocyst accumulates, and the FM4-64-labeled inverted cone of endocytotic and recycling vesicles. The PM zone showing low FM4-64 levels and high GFP-SEC3a accumulation, which was detected even following prolonged staining with FM4-64, suggests that exocyst-dependent exocytosis, which is responsible for the secretion of esterified pectins and possibly also PME and PME inhibitor, is separable from the FM4-64-labeled vesicles. These findings are compatible with data showing forward-moving Golgi-derived vesicles filled with pectins at the flanks (Chebli et al., 2013; Hepler et al., 2013). The subregion on apical PM showing low FM4-64 and high GFP-SEC3a labeling also correlates with the direction of tube elongation, strongly suggesting that extensive and focused exocytosis on the apical PM is essential for tip growth in Arabidopsis pollen (Fig. 10B). Likewise, it seems that, in addition to the well-known zonation of the tube apex to apical, subapical, and flank domains, the apical PM is farther subdivided into discrete domains of highly active exocytosis. This finding supports the model according to which, at least in Arabidopsis, growth occurs at the tip and suggests that this region might be a sensor for external signals that orient tube elongation.

Several lines of evidence indicate that both recycling and forward secretory vesicle transport are required for pollen tube growth. The GBF ADP Ribosylation Factor Guanine Nucleotide Exchange Factor (ARFGEF) family GNOM-LIKE2 (GNL2) regulates vesicle recycling. It has been shown that pollen tube growth and pectin secretion are compromised in Arabidopsis *gnl2* mutants (Richter et al., 2011). A second family of ARFGEFs called BIGs functions redundantly in secretory vesicle trafficking, and around 50% of the pollen of *big1243*$^{-/+}$ quadruple mutants fails to germinate (Richter et al., 2014), similar to *sec3a-1*. GNL2 and the BIGs regulate vesicle formation at the trans-Golgi network, while the exocyst functions in vesicle tethering at the PM and thus may function with both GNL2 and BIGs vesicle populations. GNL2 has been shown to reside in FM4-64-labeled and nonlabeled membranes (Richter et al., 2011). The spatial separation between strong PM and intracellular FM4-64 labeling and GFP-SEC3a accumulation at the tip-growing site indicates that at least part of the exocyst-dependent exocytosis might not be detected by differential labeling with both FM1-43 and FM4-64 (Zonia and Munnik, 2008). Likely, differential staining with the two FM dyes enabled the detection of vesicle recycling events but not the exocytosis of vesicles at the tip. The high density of vesicles at the pollen tube tip makes it technically difficult to separate between different vesicle populations. The exocyst only transiently associates with secretory vesicles at the PM, making GFP-SEC3a/YFP-SEC3a/SEC3a-YFP highly suitable intracellular makers for determining the sites of polarized exocytosis in pollen. Our results also indicate that it is important to image markers like FM4-64 at low laser intensity and detector gain to avoid oversaturation of the signal that can obscure the zonation at the tip. The differences in GFP-SEC3a localization, FM4-64 staining, and secretion of esterified pectins between growing and arrested pollen tubes highlight that it is critical to correlate between the localization of markers and the growth status of the pollen tube. In our hands, PI and FM4-64 compromised the growth of Arabidopsis pollen tubes, and it was critical to find suitable concentrations of the dyes that could still be imaged but have no or minimal effects on growth.

Our results in tobacco pollen tubes indicate differential localization, and hence function, of SEC3 depending on pollen tube growth mode, suggesting that different routes and membrane target domains for exocytosis may exist in pollen tubes growing continuously or in oscillatory mode (Fig. 10C). We found that, when transiently expressed in steady-growing tobacco pollen tubes, both N-terminal and C-terminal fusions of SEC3a were more enriched on the PM at the subapical region, which at first glance seemed to be different from the tip-focused localization in Arabidopsis. However, SEC3a also was dynamically localized to the cell apex in tobacco pollen tubes, showing oscillatory growth. Due to their small size, it was impossible to discern between oscillatory and steady-state growth in Arabidopsis pollen tubes, and it remains unknown whether these two growth modes exist in Arabidopsis. Hence, the differences in the distribution of SEC3a between Arabidopsis and tobacco might reflect differences in the growth modes of pollen tubes in the two systems. Also, tobacco pollen tubes are almost twice wider than Arabidopsis tubes, and change

in apical dome geometry might allow more spatial separation of functional PM regions.

Binding of SEC3a-N to Phosphoinositides and Significance of PIP_2-Dependent Interaction with the PM for SEC3a Function

Our biochemical, bioinformatics, and MD computational analyses firmly indicate that, similar to yeast Sec3p, the plant SEC3 subunit contains an N-terminal PH domain that interacts with PIP_2. Despite a clear importance of PIPs for binding of the N-terminal domain to the PM, complementation and localization analysis of the SEC3a-ΔN and SEC3a-N KRKR/A mutants in Arabidopsis pollen indicated that the interaction with PIP_2 is not absolutely required for the polar localization and function of SEC3a. Similarly, deletion of the N-terminal region of yeast Sec3p does not cause any detectable secretion or growth defects (Guo et al., 2001). Genetic analysis in yeast indicated that a dual interaction of Sec3p with phospholipids and with Cdc42 controls its function (Zhang et al., 2008). Thus, the most likely explanation for the functionality and polar localization of SEC3A N-terminal domain mutants is that additional factors regulate its association with the membrane. It is possible that such a factor is the whole exocyst complex as a functional unit. In contrast to yeast and animal cells, the interaction of SEC3a with activated ROPs is indirect, and in vegetative tissues, it is mediated by the ROP effector ICR1 (Lavy et al., 2007). Publicly available RNA expression data and ICR1 promoter-reporter fusion constructs indicate that ICR1 itself is not expressed in pollen. Therefore, a pollen-specific mechanism of putative SEC3-GTPase interaction remains to be uncovered.

A comparison of the alignment of the SEC3 N-terminal domain of various eukaryotes with our MD simulations, both presented here and recently published (Pleskot et al., 2015), revealed that some PIP_2-interacting residues are conserved among plants and fungi but not in animals. This finding is in agreement with the hypothesis that PIP_2 binding is important, but not absolutely required, for SEC3 function, as it was probably lost in the animal SEC3 genes.

Interestingly, in tobacco pollen tubes, GFP-SEC3a-N showed a somewhat stronger association with the PM compared with the full-length protein. Taking into account that SEC3a polar localization and association with the PM is highly dynamic, we can speculate that binding to phosphoinositides stabilizes the interaction of protein and the PM. Under this scenario, the distribution of PIP_2 at the tip will affect the efficiency of SEC3a recruitment to specific domains on the PM and, hence, will locally increase tethering and the subsequent fusion of secretory vesicles. Likewise, in nongrowing Arabidopsis pollen tubes, GFP-SEC3 was wider and not polarized (Figs. 3 and 10; Supplemental Movie S3), suggesting that it might have promoted diffuse rather than polarized exocytosis.

Yeast and mammalian EXO70 subunits also interact directly with PIP_2 in the membrane (He et al., 2007; Pleskot et al., 2015), and it is thus plausible to speculate that some plant EXO70 subunits bind PIP_2 or other PPIs. Therefore, in plants, the exocyst also might interact directly, via both the SEC3 and EXO70 subunits, with the specific phosphoinositide, similar to polarized and migrating animal or yeast cells (Thapa et al., 2012; Pleskot et al., 2015). In yeast cells, Sec3p missing the N-terminal PH domain is able to interact with the rest of the exocyst complex (Baek et al., 2010; Luo et al., 2014), and a similar interaction could be expected for plant SEC3a. Interestingly, Arabidopsis SEC3a interacts directly with EXO70A1 (Hála et al., 2008). Thus, the complementation of the *sec3a* mutant phenotype by SEC3a-ΔN and SEC3a-KRKR/A could be explained by the fact that mutated SEC3a is still able to interact with the other exocyst subunits, and the whole complex could be targeted by some EXO70 paralogs.

Our results also are compatible with a different scenario, under which SEC3 localization is alternately regulated by PIP_2-dependent versus PIP_2-independent mechanisms. The alternative binding of SEC3 by PIP_2-dependent and -independent mechanisms can explain the function and polar localization of SEC3a-ΔN and SEC3a KRKR/A as well as the stronger binding of SEC3a-N to the PIPs. Alternative PIP-dependent and -independent polarization mechanisms also are compatible with the differential localization of SEC3a during continuous and oscillatory growth modes in tobacco pollen tubes. Future work will be required to understand the molecular mechanisms underlying the dynamic function of the exocyst complex in relation to the exocytotic machinery under different pollen tube growth modes.

MATERIALS AND METHODS

Plant Growth Conditions

Seeds of wild-type Col-0 and mutant Arabidopsis (*Arabidopsis thaliana*) plants were sown on soil, left for 2 d at 4°C, and grown under long-day conditions (16-h-light/8-h-dark cycle) at 22°C. The light intensity was 100 μE m^{-2} s^{-1}. For segregation analysis, seedlings were surface sterilized and sown on plates containing 0.5× Murashige and Skoog salt mixture (Duchefa Biochemie) titrated to pH 5.5 with MES and KOH, 1% Suc, 0.8% plant agar (Duchefa Biochemie), and 5.25 μg mL^{-1} Sd (Duchefa Biochemie). For BASTA selection, seedlings were transferred to soil and sprayed with 0.2 g L^{-1} BASTA (Bayer CropScience).

Cloning Strategies

All primers used in this study are listed in Supplemental Table S5. For the construction of *LAT52:SEC3a/GFP-SEC3a*, *SEC3a* coding sequence flanked by attB1/attB2 sites was generated by two rounds of PCR with primers 1427/1428 and 1429/1430 and recombined into the *pDONOR221* vector (*pSY597*). *pSY597* was then used in GATEWAY LR clonase reactions with *pZO1* (untagged) and *pZO2* (N-terminal GFP fusion) destination vectors to create *pSY598* (*LAT52:SEC3a*) and *pSY599* (*LAT52:GFP-SEC3a*) expression vectors. For the construction of *LAT52:GFP-SEC3-ΔN/SEC3-ΔN*, *SEC3a* sequence without the first 540 bp was amplified by two rounds of PCR using 2546/1428 and 2547/1430 primers, recombined first into *pDONOR221* (*pSY2538*) and then recombined into *pZO1* or *pZO2* to get *pSY2539* or *pSY2540*, respectively. SEC3a promoter (*PSEC3a:GUS*) was cloned by amplifying a 1,025-bp fragment upstream of the initiation ATG codon from genomic DNA with the oligonucleotide primers SYP594 and

SYP595. The PCR product was digested with *Acc*651/*Sal*I, and the resulting fragment was subcloned into *pLhG4*-Bj36 upstream of the synthetic transcriptional factor gene *LhG4* (Moore et al., 1998) to yield *pSY581*. *pSY581* was digested with *Not*I, and the *PSEC3a-LhG4* fragment was subcloned into the plant binary vector *pART27* to yield *pSY582*. Four independent promoter lines were used for analysis. For the cloning of *LAT52:YFP-SEC3a/SEC3a-YFP*, *SEC3a* coding sequences flanked by *Ngo*MIV/*Apa*I sites were generated by PCR using Phusion DNA polymerase (Thermo Fisher) using specific primers PPP66/PPP65 (*YFP-SEC3a*), PPP66/PPP64 (*SEC3a-YFP*), PPP66/PPP63 (*YFP-SEC3a-N*), PPP66/PPP62 (*SEC3a-N-YFP*), PPP90/PPP65 (*YFP-SEC3a-ΔN*), and PPP90/PPP64 (*SEC3a-ΔN-YFP*). Amplified products were introduced into the multiple cloning sites of pollen expression vectors *pWEN240* and *pHD32* using *Ngo*MIV/*Apa*I restriction enzyme sites. The *pWEN240* vector (*LAT52:YFP-GA5-MCS:NOS*) and the *pHD32* vector (*LAT52:MCS-GA5-YFP:NOS* [Klahre et al., 2006]) were kindly provided by Benedikt Kost. These constructs allowed pollen-specific expression and visualization of SEC3a protein fusions controlled by the *LAT52* promoter (Twell et al., 1991). Multistep cloning was used to prepare *LAT52:YFP-SEC3a-N KRKR/A*. Initially, a double mutant, SEC3a-N K51A R53A, was prepared by two-step PCR. First, *SEC3a-N K51A R53A* was generated using PPP66/PPP126 primers. Next, the obtained product was used as a forward primer for a second PCR with reverse primer PPP63, and the amplified product was cloned into *pWEN240*. Then, SEC3a-N carrying a double mutation, K34A R36A, was generated using PPP66/PPP128 primers. The product was used as a forward primer for a second PCR using *YFP-SEC3a-N K51A R53A* as a template for PCR with reverse primer PPP63, and the amplified final product was cloned into *pWEN240*. *LAT52:GFP-SEC3a KRKR/A* and *SEC3a KRKR/A* were prepared by fusion reaction of two PCR products. The first product was amplified with 1427/2552 using *SEC3a-N KRKR/A* as a template, and the second product was amplified with 2553/1428 using *pSY597* as a template. The final product was then amplified with 1429/1430 and recombined into *pDONOR221* (*pSY2525*) and then into *pZO1* or *pZO2* to get *pSY2526* or *pSY2527*, respectively. For GST-SEC3a-N, the first 180 amino acids of Arabidopsis SEC3a were amplified with primers PPP129/PPP130 by PCR using Phusion DNA polymerase, digested with *Bam*HI/*Xho*I, and subcloned into the *pGEX-4T2* vector.

DNA/RNA Techniques

Genomic DNA was extracted using the GenElute Plant Genomic kit (Sigma-Aldrich) according to the manufacturer's instructions. Total RNA was isolated from seedlings, flowers, or specific tissues using the RNeasy Plus kit (Qiagen) according to the manufacturer's instructions. cDNA first-strand synthesis was carried out using the High Capacity cDNA RT kit (Applied Biosystems) with oligo(dT) primer according to the manufacturer's instructions. All PCRs were performed using PhireII DNA polymerase (Thermo Scientific). For sequencing, genomic fragments were amplified using Phusion DNA polymerase (Thermo Scientific).

GUS Staining

GUS staining was carried out as described previously (Wiegel and Glazebrook, 2002). Light imaging was performed using an Axioplan-2 Imaging microscope (Carl Zeiss) equipped with an Axio-Cam cooled CCD camera with either 10× or 20× objectives.

In Vitro Germination of Arabidopsis Pollen

Pollen from $qrt^{-/-}$ and $qrt^{-/-}$/$sec3a\text{-}1^{+/-}$ plants was germinated on 60-mm petri dishes containing pollen germination medium [1% boric acid, 5 mM $CaCl_2$, 5 mM KCl, 1 mM $MgSO_4$, 10% D-(+)-Suc, and 1.5% low-melting-point agarose, pH 7.7; Boavida and McCormick, 2007]. Pollen from seven to eight anthers was spread on a 5-mm^2 area in the middle of the dish and germinated at 22°C to 23°C for 24 h in closed plastic boxes filled with water to maintain humidity. The number of quartets showing one, two, three, or four germinated pollen grains was counted. Statistical analyses were performed using the χ^2 test.

For total RNA extraction, Col-0 pollen was germinated in 50 μL of liquid germination medium in 96 wells at 22°C to 23°C for 24 h, collected, centrifuged at 2,000*g* for 5 min, and used for total RNA extraction.

Time-Lapse Imaging and Live Staining in Arabidopsis Pollen

For live-cell imaging, pollen was germinated on solid medium as described above. Two to 3 h after plating, a piece of agar with germinated pollen was transferred to a glass-bottom 35-mm dish filled with 100 μL of liquid germination medium to prevent drying and examined using an inverted Zeiss LSM780-NLO confocal laser scanning microscope (Carl Zeiss) using Plan-Apochromat 20×/0.8 dry and C-Apochromat 40×/1.20 water objectives. GFP was exited with a 488-nm argon laser, emission was collected with a GaAsP detector set to 505 to 550 nm, with the pinhole closed to 1 Airy unit. Time-lapse images were taken in 5-s intervals for approximately 3.5 min. FM4-64 (5 mM in dimethyl sulfoxide; Invitrogen) and PI (1 mg mL^{-1} in water; Sigma-Aldrich) were diluted in germination medium, and 100 μL was applied to a piece of agar with pollen transferred to a glass-bottom dish. For simultaneous detection with GFP, FM4-64 or PI was excited with a 561-nm laser and detection was set to 580 to 650 nm in a multitrack mode, with the pinhole closed to 1 Airy unit. The GFP/FM4-64/PI signals were converted into a range of intensities using the ZEN software (Zeiss). Intensity plots for GFP/FM4-64 and GFP/PI were created by measuring the intensity of the signal for each channel across the plasma membrane of the pollen tube apex with the Fiji plot profile feature.

In Vivo Germination of Arabidopsis Pollen

Col-0 flowers were emasculated and pollinated with single quartets (approximately 10 per stigma). After 24 h, crosses were collected and fixed for 1 h in formalin-acetic alcohol, washed extensively, and transferred to 8 N NaOH solution for 12 to 36 h. In turn, germinated and fixed material was washed with water and stained with 0.05% (w/v) Aniline Blue in sodium phosphate buffer, pH 8, for 24 h. Callose staining was visualized with an epifluorescence microscope with UV light excitation and was used to count the number of germinated pollen tubes in each tetrad. Pollen tube counting was carried out directly on the microscope. Differential interference contrast images of the same tetrads were used for labeling pollen with germinating pollen tubes.

Immunolocalization of Cell Wall Pectins in Arabidopsis Pollen

For immunolocalization, pollen was germinated in a liquid germination medium [1% boric acid, 5 mM $CaCl_2$, 5 mM KCl, 1 mM $MgSO_4$, 10% D-(+)-Suc, and 1 mM $MgSO_4 \cdot 7H2O$, pH 7.7]. Pollen was isolated by submerging and vortexing approximately 40 flowers in 1 mL of germination medium. In turn, pollen was pelleted by centrifugation at 3,000*g* for 6 min, resuspended in 250 μL of germination medium, and grown in 24 wells for 4 to 5 h at 23°C with gentle agitation. Immunolocalization of cell wall epitopes was done according to the method described by Dardelle et al. (2010) with the following modifications. LM19 anti-deesterified homogalacturonan and LM20 anti-methylesterified homogalacturonan monoclonal antibodies were obtained from PlantProbes and used as primary antibodies. Both antibodies were used at a dilution of 1:10 and incubated overnight at 4°C with the pollen tubes. Goat anti-rat IgG Alexa 568 conjugated antibody (ab175710; Abcam) was used as a secondary antibody at a dilution of 1:100 to 1:200 and incubated with the pollen tubes for 3 h at 30°C. For controls, pollen tubes were incubated only with the secondary antibody.

Staining of Pollen Nuclei with DAPI

Pollen from $qrt^{-/-}$ and $qrt^{-/-}$/$sec3a\text{-}1^{+/-}$ plants was mounted on slides with 2.5% gelatin and stained for 30 min with 1 μg mL^{-1} DAPI solution.

Pollen Transformation and Microscopic Analysis in Tobacco

Expression vectors were transferred into tobacco (*Nicotiana tabacum*) pollen grains germinating on solid culture medium by particle bombardment using a particle delivery system (PDS-1000/He; Bio-Rad) as described previously (Kost et al., 1998). Particles were coated with 1 to 3 μg of DNA. When two constructs were coexpressed, particles were coated with 1 μg of each DNA. For YFP live-cell imaging, 6-h-old pollen tubes were observed using a spinning-disc confocal microscope (Yokogawa CSU-X1 on Nikon Ti-E platform) equipped with a 60× Plan Apochromat objective (WI; numerical aperture = 1.2) and an Andor Zyla sCMOS camera. Laser excitation at 488 nm together with a 542/27-nm single-band filter (Semrock Brightline) were used for fluorescence collection of YFP. Laser power and camera settings were kept constant, allowing for comparative imaging. Zeiss LSM 5 DUO CSLM in a multitrack imaging in-line switching mode was used for simultaneous detection of YFP-SEC3a-N and mRFP1-$PH_{PLC\delta1}$ fluorescence using the Zeiss C-Apochromat 40×/1.2 water-corrected

objective. YFP-SEC3a-N excited with the 488-nm laser was imaged through a 405/488/561-nm dichroic and a 505- to 550-nm band-pass emission filter. Laser line 561 nm was used to excite mRFP1-$PH_{PLC\delta1}$, which was imaged through a 405/488/561-nm dichroic and a 575-nm long-pass emission filter. For comparative imaging of *LAT52:YFP-SEC3a-N KRKR/A* and wild-type *LAT52:YFP-SEC3a-N*, gain and offset detector settings were kept constant.

Expression of Recombinant GST-SEC3a-N, Purification, and Lipid-Binding Assays

The expression plasmid coding for GST-SEC3a-N was transformed into *Escherichia coli* strain BL21, and cells were grown overnight at 37°C. After subculturing into fresh medium, cells were grown at 37°C to an optical density at 600 nm of 1.5, then induced for 4 h using 0.4 mM isopropylthio-β-galactoside. Recombinant proteins were purified on glutathione-Sepharose (GE Healthcare) according to the manufacturer's instructions. Protein-lipid overlay assays with membrane lipid strips (Echelon Biosciences P-6002) were performed according to the manufacturer's instructions with protein concentration of 0.5 μg mL^{-1}. For the large unilamellar vesicle cosedimentation assay, we used the procedure described by Kooijman et al. (2007) using 400 nmol of lipids and 1 μg of GST-SEC3a-N.

Homology Model of Arabidopsis SEC3a-N

A homology model for Arabidopsis SEC3a-N was constructed using the ScSec3p-N structure (3A58). The manually edited alignment obtained by PSIPRED (Buchan et al., 2010) was used as an input for MODELER-9v8 (Sali and Blundell, 1993). The loop refinement method of the MODELER program was utilized to model the 10-amino acid-long loop in SEC3a-N (region 110–119). The best model was evaluated by the ProSA and WHAT IF algorithms (Vriend, 1990).

MD Simulations

To simulate the self-assembly of lipid bilayers in the presence of protein, the MARTINI CG force field was used (Marrink et al., 2007; Monticelli et al., 2008). We simulated two systems, the first containing SEC3a-N, one molecule of PIP_2, 255 molecules of PC, CG waters, and chloride ions and the second comprising AtSEC3a-N, 256 molecules of PC, CG waters, and chloride ions. The protein was described according to ELNEDYN representation (Periole et al., 2009) with Rc of 0.9 nm and K (spring force constant) of 500 kJ mol^{-1} nm^{-2}. GROMACS 4.0.5 was used for all MD simulations (Hess et al., 2008). The simulation conditions were used according to Pleskot et al. (2012). Systems were energy minimized using the steepest descent method up to a maximum of 500 steps, and production runs for 16 μs were performed. It was shown that effective (real) times for CG simulations are longer (cut-off distance) than computational ones; for proteins and lipids in the MARTINI force field, the scaling factor is 4-fold (Ramadurai et al., 2010; i.e. a 4-μs simulation time corresponds to 16 μs of real time). The snapshots from MD simulations were prepared using VMD (Humphrey et al., 1996).

Accession Numbers

Accession numbers are as follows: SEC3a, At1g47550; and SEC3b, At1g47560.

Supplemental Data

The following supplemental materials are available.

Supplemental Figure S1. Schematic representation of *SEC3a* and *SEC3b* mRNA coding sequences and 3′ untranslated regions.

Supplemental Figure S2. Genotyping of *sec3a-1* and *sec3b-1*.

Supplemental Figure S3. Phenotype of the *sec3b-1* homozygote.

Supplemental Figure S4. Pollen nuclei display similar staining in *qrt*$^{-/-}$ and *qrt*$^{-/-}$ *sec3a*$^{-/+}$ single and double mutants.

Supplemental Figure S5. Distribution of FM4-64 in growing nontransgenic Col-0 pollen tubes.

Supplemental Figure S6. Nongrowing Arabidopsis pollen tube labeled with FM4-64.

Supplemental Figure S7. Localization of Arabidopsis and tobacco SEC3a variants in tobacco pollen tubes.

Supplemental Figure S8. Phylogenetic analysis of SEC3 N-terminal domain and SEC3 domain.

Supplemental Figure S9. Multiple sequence alignment of SEC3 N-terminal domain for selected organisms.

Supplemental Table S1. Reciprocal outcrosses of *sec3a-1*$^{-/+}$ and first progeny of *LAT52::SEC3a* and *LAT52::GFP-SEC3a* complementation lines to the Col-0 background.

Supplemental Table S2. Segregation of *sec3a-1*$^{+/-}$ mutant and complementation lines based on Sd resistance.

Supplemental Table S3. Abortion of seed development in the *sec3a-1* heterozygote.

Supplemental Table S4. Outcrosses of *sec3a-1*$^{+/-}$*/LAT52::SEC3a* KRKR/A, *sec3a-1*$^{+/-}$*/LAT52::GFP-SEC3a* KRKR/A, *sec3a-1*$^{+/-}$*/LAT52::SEC3a-*ΔN$^{+/-}$, and *sec3a-1*$^{+/-}$*/LAT52::GFPSEC3a-*ΔN$^{+/-}$ complementation lines to Col-0.

Supplemental Table S5. Primers used in this study.

Supplemental Movie S1. Localization of GFP-SEC3a in growing Arabidopsis pollen tube.

Supplemental Movie S2. Localization of GFP-SEC3a in growing Arabidopsis pollen tube.

Supplemental Movie S3. Localization of GFP-SEC3a in nongrowing Arabidopsis pollen tube.

Supplemental Movie S4. Localization of GFP-SEC3a in multiple-tip *sec3a*$^{-/-}$*;GFPSEC3a* pollen.

Supplemental Movie S5. Localization of GFP-SEC3a in multiple-tip *sec3a*$^{-/-}$*;GFPSEC3a* pollen.

Supplemental Movie S6. Localization of GFP-SEC3a KRKR/A in growing Arabidopsis pollen tube.

Supplemental Movie S7. Localization of GFP-SEC3a KRKR/A in nongrowing (first 5 min) pollen tube that starts to grow (GFP-SEC3a KRKR/A defines that position of growth).

Supplemental Movie S8. Localization of *GFP-sec3a-*ΔN in growing Arabidopsis pollen tube.

Supplemental Movie S9. Localization of *GFP-sec3a-*ΔN in growing Arabidopsis pollen tube.

ACKNOWLEDGMENTS

We thank Benedikt Kost (University of Erlangen-Nuremberg) for providing us the *LAT52:mRFP1:*$PH_{PLC\delta1}$ construct and the developers of the Linux operation system and other open-source programs used in the preparation of this study, particularly Gimp, Gnumeric, GROMACS, Inkscape, and ImageJ.

Received July 14, 2016; accepted August 8, 2016; published August 11, 2016.

LITERATURE CITED

Baek K, Knödler A, Lee SH, Zhang X, Orlando K, Zhang J, Foskett TJ, Guo W, Dominguez R (2010) Structure-function study of the N-terminal domain of exocyst subunit Sec3. J Biol Chem **285:** 10424–10433

Boavida LC, McCormick S (2007) Temperature as a determinant factor for increased and reproducible in vitro pollen germination in Arabidopsis thaliana. Plant J **52:** 570–582

Bove J, Vaillancourt B, Kroeger J, Hepler PK, Wiseman PW, Geitmann A (2008) Magnitude and direction of vesicle dynamics in growing pollen tubes using spatiotemporal image correlation spectroscopy and fluorescence recovery after photobleaching. Plant Physiol **147:** 1646–1658

Buchan DW, Ward SM, Lobley AE, Nugent TC, Bryson K, Jones DT (2010) Protein annotation and modelling servers at University College London. Nucleic Acids Res **38:** W563–W568

Chebli Y, Geitmann A (2007) Mechanical principles governing pollen tube growth. Funct Plant Sci Biotechnol **1:** 232–245

Chebli Y, Kaneda M, Zerzour R, Geitmann A (2012) The cell wall of the Arabidopsis pollen tube: spatial distribution, recycling, and network formation of polysaccharides. Plant Physiol **160:** 1940–1955

Chebli Y, Kroeger J, Geitmann A (2013) Transport logistics in pollen tubes. Mol Plant **6:** 1037–1052

Cheung AY, Wu HM (2008) Structural and signaling networks for the polar cell growth machinery in pollen tubes. Annu Rev Plant Biol **59:** 547–572

Cole RA, Synek L, Zarsky V, Fowler JE (2005) SEC8, a subunit of the putative Arabidopsis exocyst complex, facilitates pollen germination and competitive pollen tube growth. Plant Physiol **138:** 2005–2018

Cvrčková F, Grunt M, Bezvoda R, Hála M, Kulich I, Rawat A, Zárský V (2012) Evolution of the land plant exocyst complexes. Front Plant Sci **3:** 159

Dardelle F, Lehner A, Ramdani Y, Bardor M, Lerouge P, Driouich A, Mollet JC (2010) Biochemical and immunocytological characterizations of Arabidopsis pollen tube cell wall. Plant Physiol **153:** 1563–1576

Derksen J, Rutten T, Lichtscheidl IK, De Win AHN, Pierson ES, Rongen G (1995) Quantitative analysis of the distribution of organelles in tobacco pollen tubes: implications for exocytosis and endocytosis. Protoplasma **188:** 267–276

Elias M, Drdova E, Ziak D, Bavlnka B, Hala M, Cvrckova F, Soukupova H, Zarsky V (2003) The exocyst complex in plants. Cell Biol Int **27:** 199–201

Fendrych M, Synek L, Pecenková T, Toupalová H, Cole R, Drdová E, Nebesárová J, Sedinová M, Hála M, Fowler JE, et al (2010) The *Arabidopsis* exocyst complex is involved in cytokinesis and cell plate maturation. Plant Cell **22:** 3053–3065

Guan Y, Guo J, Li H, Yang Z (2013) Signaling in pollen tube growth: crosstalk, feedback, and missing links. Mol Plant **6:** 1053–1064

Guo W, Grant A, Novick P (1999) Exo84p is an exocyst protein essential for secretion. J Biol Chem **274:** 23558–23564

Guo W, Tamanoi F, Novick P (2001) Spatial regulation of the exocyst complex by Rho1 GTPase. Nat Cell Biol **3:** 353–360

Hála M, Cole R, Synek L, Drdová E, Pecenková T, Nordheim A, Lamkemeyer T, Madlung J, Hochholdinger F, Fowler JE, et al (2008) An exocyst complex functions in plant cell growth in *Arabidopsis* and tobacco. Plant Cell **20:** 1330–1345

He B, Guo W (2009) The exocyst complex in polarized exocytosis. Curr Opin Cell Biol **21:** 537–542

He B, Xi F, Zhang X, Zhang J, Guo W (2007) Exo70 interacts with phospholipids and mediates the targeting of the exocyst to the plasma membrane. EMBO J **26:** 4053–4065

Helling D, Possart A, Cottier S, Klahre U, Kost B (2006) Pollen tube tip growth depends on plasma membrane polarization mediated by tobacco PLC3 activity and endocytic membrane recycling. Plant Cell **18:** 3519–3534

Hepler PK, Rounds CM, Winship LJ (2013) Control of cell wall extensibility during pollen tube growth. Mol Plant **6:** 998–1017

Hepler PK, Winship LJ (2015) The pollen tube clear zone: clues to the mechanism of polarized growth. J Integr Plant Biol **57:** 79–92

Hess B, Kutzner C, van der Spoel D, Lindahl E (2008) GROMACS 4: algorithms for highly efficient, load-balanced, and scalable molecular simulation. J Chem Theory Comput **4:** 435–447

Humphrey W, Dalke A, Schulten K (1996) VMD: visual molecular dynamics. J Mol Graph **14:** 33–38

Idilli AI, Morandini P, Onelli E, Rodighiero S, Caccianiga M, Moscatelli A (2013) Microtubule depolymerization affects endocytosis and exocytosis in the tip and influences endosome movement in tobacco pollen tubes. Mol Plant **6:** 1109–1130

Jafar-Nejad H, Andrews HK, Acar M, Bayat V, Wirtz-Peitz F, Mehta SQ, Knoblich JA, Bellen HJ (2005) Sec15, a component of the exocyst, promotes notch signaling during the asymmetric division of Drosophila sensory organ precursors. Dev Cell **9:** 351–363

Klahre U, Becker C, Schmitt AC, Kost B (2006) Nt-RhoGDI2 regulates Rac/Rop signaling and polar cell growth in tobacco pollen tubes. Plant J **46:** 1018–1031

Kooijman EE, Tieleman DP, Testerink C, Munnik T, Rijkers DT, Burger KN, de Kruijff B (2007) An electrostatic/hydrogen bond switch as the basis for the specific interaction of phosphatidic acid with proteins. J Biol Chem **282:** 11356–11364

Kost B, Spielhofer P, Chua NH (1998) A GFP-mouse talin fusion protein labels plant actin filaments in vivo and visualizes the actin cytoskeleton in growing pollen tubes. Plant J **16:** 393–401

Kulich I, Cole R, Drdová E, Cvrcková F, Soukup A, Fowler J, Zárský V (2010) Arabidopsis exocyst subunits SEC8 and EXO70A1 and exocyst interactor ROH1 are involved in the localized deposition of seed coat pectin. New Phytol **188:** 615–625

Lamesch P, Berardini TZ, Li D, Swarbreck D, Wilks C, Sasidharan R, Muller R, Dreher K, Alexander DL, Garcia-Hernandez M, et al (2012) The Arabidopsis Information Resource (TAIR): improved gene annotation and new tools. Nucleic Acids Res **40:** D1202–D1210

Lancelle SA, Cresti M, Hepler PK (1987) Ultrastructure of the cytoskeleton in freeze-substituted pollen tubes of Nicotiana alata. Protoplasma **140:** 141–150

Lancelle SA, Hepler PK (1992) Ultrastructure of freeze-substituted pollen tubes of Lilium longiflorum. Protoplasma **167:** 215–230

Lavy M, Bloch D, Hazak O, Gutman I, Poraty L, Sorek N, Sternberg H, Yalovsky S (2007) A novel ROP/RAC effector links cell polarity, root-meristem maintenance, and vesicle trafficking. Curr Biol **17:** 947–952

Lemmon MA (2008) Membrane recognition by phospholipid-binding domains. Nat Rev Mol Cell Biol **9:** 99–111

Leroux C, Bouton S, Kiefer-Meyer MC, Fabrice TN, Mareck A, Guénin S, Fournet F, Ringli C, Pelloux J, Driouich A, et al (2015) PECTIN METHYLESTERASE48 is involved in Arabidopsis pollen grain germination. Plant Physiol **167:** 367–380

Lin Y, Ding Y, Wang J, Shen J, Kung CH, Zhuang X, Cui Y, Yin Z, Xia Y, Lin H, et al (2015) Exocyst-positive organelles and autophagosomes are distinct organelles in plants. Plant Physiol **169:** 1917–1932

Liu SL, Baute GJ, Adams KL (2011) Organ and cell type-specific complementary expression patterns and regulatory neofunctionalization between duplicated genes in Arabidopsis thaliana. Genome Biol Evol **3:** 1419–1436

Luo G, Zhang J, Guo W (2014) The role of Sec3p in secretory vesicle targeting and exocyst complex assembly. Mol Biol Cell **25:** 3813–3822

Marrink SJ, Risselada HJ, Yefimov S, Tieleman DP, de Vries AH (2007) The MARTINI force field: coarse grained model for biomolecular simulations. J Phys Chem B **111:** 7812–7824

McKenna ST, Kunkel JG, Bosch M, Rounds CM, Vidali L, Winship LJ, Hepler PK (2009) Exocytosis precedes and predicts the increase in growth in oscillating pollen tubes. Plant Cell **21:** 3026–3040

Mehta SQ, Hiesinger PR, Beronja S, Zhai RG, Schulze KL, Verstreken P, Cao Y, Zhou Y, Tepass U, Crair MC, et al (2005) Mutations in Drosophila sec15 reveal a function in neuronal targeting for a subset of exocyst components. Neuron **46:** 219–232

Monticelli L, Kandasamy SK, Periole X, Larson RG, Tieleman DP, Marrink SJ (2008) The MARTINI coarse-grained force field: extension to proteins. J Chem Theory Comput **4:** 819–834

Moore I, Galweiler L., Grosskopf D, Schell J, Palme K (1998) A transcription activation system for regulated gene expression in transgenic plants. Proc Natl Acad Sci USA **95:** 376–381

Moscatelli A, Idilli AI, Rodighiero S, Caccianiga M (2012) Inhibition of actin polymerisation by low concentration latrunculin B affects endocytosis and alters exocytosis in shank and tip of tobacco pollen tubes. Plant Biol (Stuttg) **14:** 770–782

Oda Y, Iida Y, Nagashima Y, Sugiyama Y, Fukuda H (2015) Novel coiled-coil proteins regulate exocyst association with cortical microtubules in xylem cells via the conserved oligomeric Golgi-complex 2 protein. Plant Cell Physiol **56:** 277–286

Pecenková T, Hála M, Kulich I, Kocourková D, Drdová E, Fendrych M, Toupalová H, Zársky V (2011) The role for the exocyst complex subunits Exo70B2 and Exo70H1 in the plant-pathogen interaction. J Exp Bot **62:** 2107–2116

Periole X, Cavalli M, Marrink SJ, Ceruso MA (2009) Combining an elastic network with a coarse-grained molecular force field: structure, dynamics, and intermolecular recognition. J Chem Theory Comput **5:** 2531–2543

Pleskot R, Cwiklik L, Jungwirth P, Žárský V, Potocký M (2015) Membrane targeting of the yeast exocyst complex. Biochim Biophys Acta **1848:** 1481–1489

Pleskot R, Pejchar P, Žárský V, Staiger CJ, Potocký M (2012) Structural insights into the inhibition of actin-capping protein by interactions with phosphatidic acid and phosphatidylinositol (4,5)-bisphosphate. PLOS Comput Biol **8:** e1002765

Preuss D, Rhee SY, Davis RW (1994) Tetrad analysis possible in Arabidopsis with mutation of the QUARTET (QRT) genes. Science **264:** 1458–1460

Ramadurai S, Holt A, Schäfer LV, Krasnikov VV, Rijkers DT, Marrink SJ, Killian JA, Poolman B (2010) Influence of hydrophobic mismatch and amino acid composition on the lateral diffusion of transmembrane peptides. Biophys J **99:** 1447–1454

Richter S, Kientz M, Brumm S, Nielsen ME, Park M, Gavidia R, Krause C, Voss U, Beckmann H, Mayer U, et al (2014) Delivery of endocytosed proteins to the cell-division plane requires change of pathway from recycling to secretion. eLife **3:** e02131

Richter S, Muller LM, Stierhof YD, Mayer U, Takada N, Kost B, Vieten A, Geldner N, Koncz C, Jurgens G (2011) Polarized cell growth in Arabidopsis requires endosomal recycling mediated by GBF1-related ARF exchange factors. Nat Cell Biol **14:** 80–86

Röckel N, Wolf S, Kost B, Rausch T, Greiner S (2008) Elaborate spatial patterning of cell-wall PME and PMEI at the pollen tube tip involves PMEI endocytosis, and reflects the distribution of esterified and de-esterified pectins. Plant J **53:** 133–143

Rojas ER, Hotton S, Dumais J (2011) Chemically mediated mechanical expansion of the pollen tube cell wall. Biophys J **101:** 1844–1853

Rounds CM, Hepler PK, Winship LJ (2014) The apical actin fringe contributes to localized cell wall deposition and polarized growth in the lily pollen tube. Plant Physiol **166:** 139–151

Safavian D, Goring DR (2013) Secretory activity is rapidly induced in stigmatic papillae by compatible pollen, but inhibited for self-incompatible pollen in the Brassicaceae. PLoS ONE **8:** e84286

Safavian D, Zayed Y, Indriolo E, Chapman L, Ahmed A, Goring DR (2015) RNA silencing of exocyst genes in the stigma impairs the acceptance of compatible pollen in Arabidopsis. Plant Physiol **169:** 2526–2538

Sali A, Blundell TL (1993) Comparative protein modelling by satisfaction of spatial restraints. J Mol Biol **234:** 779–815

Sanati Nezhad A, Packirisamy M, Geitmann A (2014) Dynamic, high precision targeting of growth modulating agents is able to trigger pollen tube growth reorientation. Plant J **80:** 185–195

Silva PA, Ul-Rehman R, Rato C, Di Sansebastiano GP, Malhó R (2010) Asymmetric localization of Arabidopsis SYP124 syntaxin at the pollen tube apical and sub-apical zones is involved in tip growth. BMC Plant Biol **10:** 179

Synek L, Schlager N, Eliás M, Quentin M, Hauser MT, Zárský V (2006) AtEXO70A1, a member of a family of putative exocyst subunits specifically expanded in land plants, is important for polar growth and plant development. Plant J **48:** 54–72

TerBush DR, Maurice T, Roth D, Novick P (1996) The exocyst is a multiprotein complex required for exocytosis in Saccharomyces cerevisiae. EMBO J **15:** 6483–6494

Thapa N, Sun Y, Schramp M, Choi S, Ling K, Anderson RA (2012) Phosphoinositide signaling regulates the exocyst complex and polarized integrin trafficking in directionally migrating cells. Dev Cell **22:** 116–130

Twell D, Yamaguchi J, Wing RA, Ushiba J, McCormick S (1991) Promoter analysis of genes that are coordinately expressed during pollen development reveals pollen-specific enhancer sequences and shared regulatory elements. Genes Dev **5:** 496–507

Verhertbruggen Y, Marcus SE, Haeger A, Ordaz-Ortiz JJ, Knox JP (2009) An extended set of monoclonal antibodies to pectic homogalacturonan. Carbohydr Res **344:** 1858–1862

Vriend G (1990) WHAT IF: a molecular modeling and drug design program. J Mol Graph **8:** 52–56

Wang J, Ding Y, Wang J, Hillmer S, Miao Y, Lo SW, Wang X, Robinson DG, Jiang L (2010) EXPO, an exocyst-positive organelle distinct from multivesicular endosomes and autophagosomes, mediates cytosol to cell wall exocytosis in *Arabidopsis* and tobacco cells. Plant Cell **22:** 4009–4030

Wen TJ, Hochholdinger F, Sauer M, Bruce W, Schnable PS (2005) The roothairless1 gene of maize encodes a homolog of sec3, which is involved in polar exocytosis. Plant Physiol **138:** 1637–1643

Wen TJ, Schnable PS (1994) Analyses of mutants of 3 genes that influence root hair development in Zea mays (Gramineae) suggest that root hairs are dispensable. Am J Bot **81:** 833–842

Wiederkehr A, De Craene JO, Ferro-Novick S, Novick P (2004) Functional specialization within a vesicle tethering complex: bypass of a subset of exocyst deletion mutants by Sec1p or Sec4p. J Cell Biol **167:** 875–887

Wiederstein M, Sippl MJ (2007) ProSA-web: interactive web service for the recognition of errors in three-dimensional structures of proteins. Nucleic Acids Res **35:** W407–W410

Wiegel D, Glazebrook J (2002) Arabidopsis: A Laboratory Manual. Cold Spring Harbor Laboratory Press, Cold Spring Harbor, NY

Wu J, Tan X, Wu C, Cao K, Li Y, Bao Y (2013) Regulation of cytokinesis by exocyst subunit SEC6 and KEULE in Arabidopsis thaliana. Mol Plant **6:** 1863–1876

Yamashita M, Kurokawa K, Sato Y, Yamagata A, Mimura H, Yoshikawa A, Sato K, Nakano A, Fukai S (2010) Structural basis for the Rho- and phosphoinositide-dependent localization of the exocyst subunit Sec3. Nat Struct Mol Biol **17:** 180–186

Zhang C, Brown MQ, van de Ven W, Zhang ZM, Wu B, Young MC, Synek L, Borchardt D, Harrison R, Pan S, et al (2016) Endosidin2 targets conserved exocyst complex subunit EXO70 to inhibit exocytosis. Proc Natl Acad Sci USA **113:** E41–E50

Zhang X, Bi E, Novick P, Du L, Kozminski KG, Lipschutz JH, Guo W (2001) Cdc42 interacts with the exocyst and regulates polarized secretion. J Biol Chem **276:** 46745–46750

Zhang X, Orlando K, He B, Xi F, Zhang J, Zajac A, Guo W (2008) Membrane association and functional regulation of Sec3 by phospholipids and Cdc42. J Cell Biol **180:** 145–158

Zhang Y, Immink R, Liu CM, Emons AM, Ketelaar T (2013) The Arabidopsis exocyst subunit SEC3A is essential for embryo development and accumulates in transient puncta at the plasma membrane. New Phytol **199:** 74–88

Zonia L, Munnik T (2008) Vesicle trafficking dynamics and visualization of zones of exocytosis and endocytosis in tobacco pollen tubes. J Exp Bot **59:** 861–873